RSC Advances

PAPER

View Article Online
View Journal | View Issue

Cite this: *RSC Adv.*, 2023, **13**, 27363

Design, green synthesis, and quorum sensing quenching potential of novel 2-oxo-pyridines containing a thiophene/furan scaffold and targeting a *Las*R gene on *P. aeruginosa*†

Yousry A. Ammar,‡[a] Ahmed Ragab, ‡*[a] M. A. Migahed,[b] S. Al-Sharbasy,[c] Mohamed A. Salem,*[d] Omnia Karem M. Riad,*[e] Heba Mohammed Refat M. Selim,*[ef] Gehad A. Abd-elmaksoud[c] and Moustafa S. Abusaif[a]

The current trend in fighting bacteria is attacking the virulence and quorum-sensing (QS) signals that control bacterial communication and virulence factors, especially biofilm formation. This study reports new Schiff bases and tetracyclic rings based on a pyridine pharmacophore by two methods: a green approach using CAN and a conventional method. The structure of designed derivatives was confirmed using different spectroscopies (IR and $^{1}H/^{13}C$ NMR) and elemental analysis. The designed derivatives exhibited good to moderate inhibition zones against bacterial and fungal pathogens. In addition, six compounds **2a,b**, **3a,b**, and **6a,b** displayed potency against tested pathogens with eligible MIC and MBC values compared to standard antimicrobial agents. Compound **2a** displayed MIC values of 15.6 μg mL^{-1} compared to Gentamicin (MIC = 250 μg mL^{-1} against *K. pneumoniae*), while compound **6b** exhibited super-potent activity against *P. aeruginosa*, and *K. pneumoniae* with MIC values of 62.5 and 125 μg mL^{-1}, as well as MBC values of 31.25 and 15.6 μg mL^{-1} compared to Gentamicin (MIC = 250 and 125 μg mL^{-1} and MBC = 62.5 μg mL^{-1}), respectively. Surprisingly, these six derivatives revealed bactericidal and fungicidal potency and remarkable anti-biofilm activity that could significantly reduce the biofilm formation against MRSA, *E. coli*, *P. aeruginosa*, and *C. albicans*. Furthermore, the most active derivatives reduced the *Las*R gene's production between 10–40% at 1/8 MICs compared with untreated *P. aeruginosa*. Besides, they demonstrated promising safety profile on Vero cells (normal cell lines) with IC_{50} values ranging between (175.17 ± 3.49 to 344.27 ± 3.81 μg mL^{-1}). In addition, the *in silico* ADMET prediction was carried out and the results revealed that these compounds could be used with oral bioavailability with low toxicity prediction when administered as a candidate drug. Finally, the molecular docking simulation was performed inside *Las*R and predicted the key binding interactions responsible for the activity that corroborated the biological results.

Received 23rd June 2023
Accepted 7th September 2023

DOI: 10.1039/d3ra04230h

rsc.li/rsc-advances

1. Introduction

Bacterial infections impose a burden on the public health system, and this issue has been exacerbated by the excessive use of antibiotics, leading to the emergence of multidrug-resistant bacterial strains (MDR).[1,2] Each year, over 700 000 people lose their lives as a result of drug-resistant strains, and if this current rate continues to increase, it might rise to be 10 million per year.[3,4] Humans spend more time in contact with microorganisms in their daily lives, leading to life-threatening infectious diseases caused by multidrug-resistant bacterial and fungal pathogens.[5,6]

In general, antibiotics and anti-infective medications are commonly used to treat microbial infections by different modes of action with the ability to inhibit or stop the growth of pathogenic bacteria through inhibiting many factors such as protein

[a]*Department of Chemistry, Faculty of Science (boys), Al-Azhar University, 11884 Nasr City, Cairo, Egypt. E-mail: ahmed_ragab@azhar.edu.eg; ahmed_ragab7@ymail.com*
[b]*Egyptian Petroleum Research Institute (EPRI), 11727 Nasr City, Cairo, Egypt*
[c]*Department of Chemistry, Faculty of Science (girls), Al-Azhar University, 11884 Nasr City, Cairo, Egypt*
[d]*Department of Chemistry, Faculty of Science and Arts, King Khalid University, Mohail, Assir, Saudi Arabia. E-mail: masalem@kku.edu.sa*
[e]*Department of Microbiology and Immunology, Faculty of Pharmacy (Girls), Al-Azhar University, Nasr City, Cairo, Egypt. E-mail: dr_omniakarem@azhar.edu.eg; hebarefat1983@gmail.com*
[f]*Department of Pharmaceutical Sciences, Faculty of Pharmacy, Al-Maarefa University, Diriyah, 13713, Riyadh, Saudi Arabia*

† Electronic supplementary information (ESI) available. See DOI: https://doi.org/10.1039/d3ra04230h

‡ These authors contributed equally as first author.

and nucleic acids synthesis, cell membrane synthesis, ATP synthase, metabolic pathway, and membrane function and so on.[7–9] Evaluating the potential for biofilm formation and antibiotic resistance is also essential for understanding the epidemiology of the disease and, as a result, establishing appropriate preventative and management strategies for the local environment.[10,11] In biofilms, bacterial cells adhere to biotic and abiotic surfaces and form an organic polymeric matrix, the exopolysaccharide, surrounding them.[12,13] These structures provide bacteria defense against antibiotics, ultraviolet radiation, dehydration, oxidation, environmental stresses, and immune responses from the host.[14,15] *In vitro* studies have shown that both pathogenic and saprophytic microorganisms *e.g.*, *leptospires* are capable of forming biofilms.[16] Moreover, several studies have observed bacterial aggregates in mammalian hosts' proximal renal tubules,[17,18] and enhanced biofilm formation in the presence of catheters.[19]

The *Pseudomonas aeruginosa* is one of the serious pathogens that develops resistance to almost all known conventional antimicrobial drugs, the human population is now in extreme danger, especially immune-compromised patients.[20,21] There is an increasing need to develop numerous antibiotics to overcome the worrisome rise in resistant bacterial infections.[22] Targeting infectious agents' virulence is a modern strategy that is getting much attention for combating antibiotic resistance.[23] Using anti-virulence tactics that interfere with bacterial quorum sensing (QS) processes is feasible. QS is the capacity to detect the density of nearby microorganisms (of the same or different

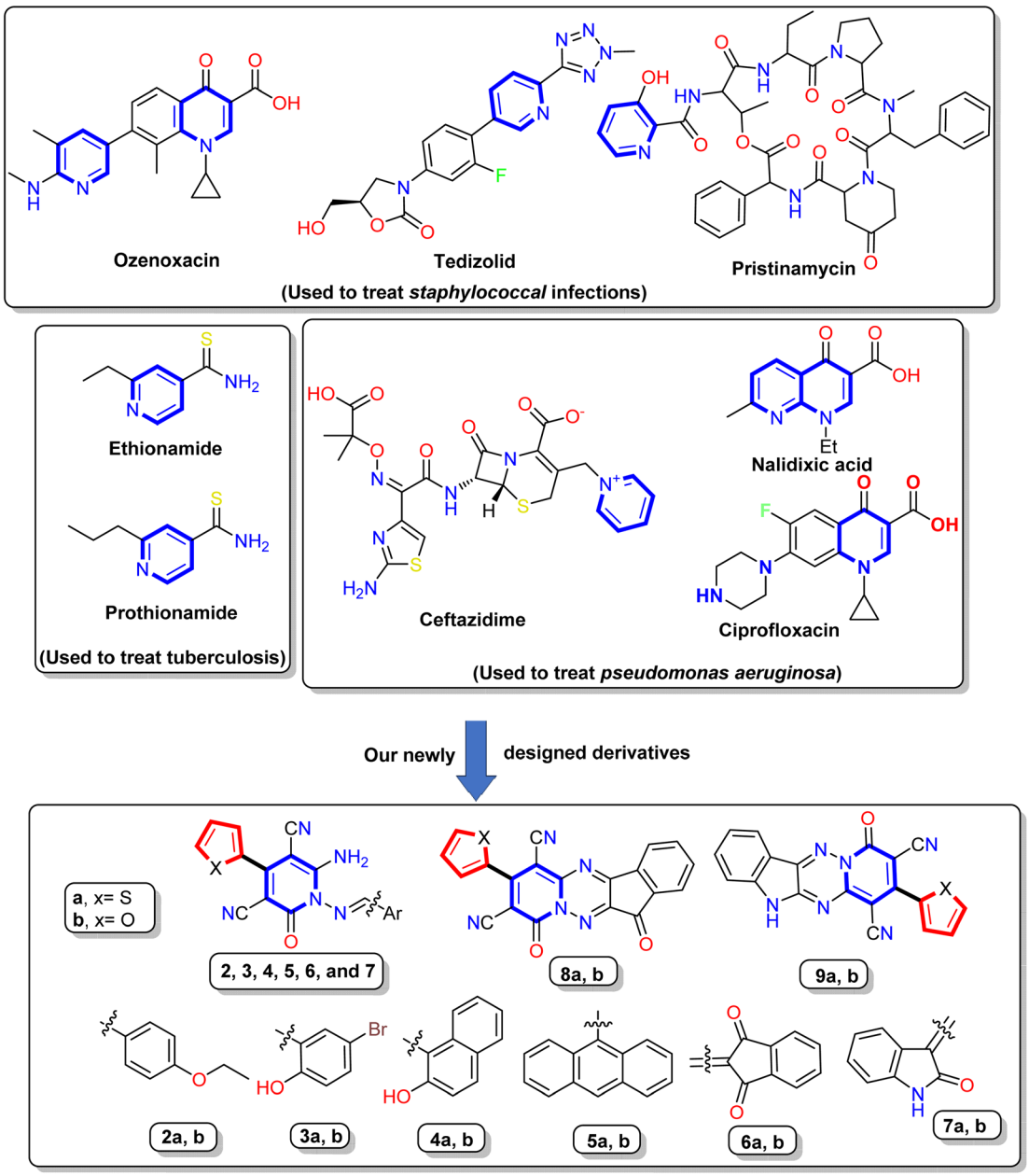

Fig. 1 Reported antibiotics containing pyridine nucleus and our newly designed derivatives.

species); hence it is responsible for bacterial communication and virulence, especially biofilm formation.[24] System heterogeneities, which are variations in the physical or chemical environment, significantly impact the ability of QS systems to coordinate gene expression and behavior.[24,25] QS and biofilm formation are highly affected by heterogeneous conditions, including nutrients and growth media, bacterial numbers, and even the constant flow that can wash autoinducers away, thus attenuating QS.[26]

As QS is mediated by autoinducers released from bacterial cells for communication, targeting signaling pathways, such as the transcriptional proteins; transcriptional regulators (*Las*R, *Rhl*R), Pseudomonas quinolone signal (Pqs), and quorum-sensing-control repressor (QScR), would aid in inhibiting the QS circuit of *P. aeruginosa*, to diminish bacterial pathogenicity.[27] *Las*R is an auto-inducer gene related to QS that can affect virulence in *P. aeruginosa*.[28] *Las*R binds specifically to DNA sequences to activate genes involved in virulence and biofilm development.[29] Inhibition of *Las*R activity can reduce the expression of virulence factors and other pathogenic traits in *P. aeruginosa*. Several antibiotics have been investigated for their potential to inhibit quorum sensing in *P. aeruginosa* by targeting *Las*R, such as Ciprofloxacin, halogenated furanone, and Azithromycin.[30]

In recent years, nitrogen heterocycles have gained increasing attention because of their diverse pharmacological and biological properties.[31] Among these nitrogenous compounds, pyridine is a widely distributed nucleus in the vitamin B6 coenzyme family, several alkaloids, and many drugs. The pyridine derivatives exhibited many activities, such as anti-oxidation, anti-inflammation, and anti-microbial defense.[32] In addition, the pyridinone nucleus displayed in a numerous of drugs, such as Gimeracil (DPD inhibitor that used in treatment of cancer), Deferiprone (an iron chelator), Pirfenidone (antifibrotic agent used to treat idiopathic pulmonary fibrosis (IPF)), Doravirine (a drug used to treat HIV), and Ciclopirox (broad spectrum antifungal agent).[33–36] Interest is increased toward antibiotics containing the pyridine nucleus, such as Pristinamycin, Ozenoxacin, and Tedizolid (used to treat *Staphylococcal* infections), Prothionamide and Ethionamide (used to treat tuberculosis (TB)), Nalidixic acid, Levofloxacin, Ciprofloxacin, and Ceftazidime (used to treat *Pseudomonas aeruginosa* infections)[37–39] Fig. 1.

Furthermore, cyanopyridone is a fundamental structural component in many organic and synthetic compounds that exhibit potential as antibacterial,[40] anti-inflammatory,[41] and antioxidant properties.[42] Subsequently, it has been shown that 3-cyano-2-oxo-pyridines can induce a variety of biological actions, such as antidepressant,[43] antibacterial,[44] and cardiotonic.[45] Besides, the Milrinone and Olprinone are well-known medications available on the market and are utilized in treating congestive heart failure.[46] Moreover, Schiff bases compounds exhibit various biological actions, including antibacterial, anticancer, antimalarial, anti-inflammatory, antioxidant, analgesic, antiviral, antifungal,[47–49] and free radical scavenging capabilities.[50]

As described in the above findings, the authors in this work aimed to synthesize a new novel *N*-amino pyridinone Schiff's base and tetracyclic structures known as indeno[1,2-*e*]pyrido[1,2-*b*][1,2,4]triazine and pyrido[1′,2′:2,3][1,2,4]triazino[5,6-*b*]indole derivatives using ceric ammonium nitrate (CAN-catalyst) and conventional method. The synthesized compounds were screened for their antibacterial and antifungal activities against seven standard microbial strains, including two Gram-positive bacteria, four standard Gram-negative strains, and one fungal isolate (*Candida albicans*) by well diffusion, MIC, and MBC methods. To evaluate the anti-virulence and anti-QS activity of the most active compounds, the microtiter plate method was used to determine the biofilm inhibitory activity. Moreover, the real-time polymerase chain reaction (real-time PCR) was used to assess their ability to decrease the expression of *Las*R gene, the key regulatory gene for QS in *P. aeruginosa*. Besides, the cytotoxic activity against normal cell line (Vero cells) was assessed to ensure the safety of the synthesized compounds. The potential *Las*R inhibitory activity was examined using *in silico* molecular docking simulation. Besides, the *in silico* drug-likeness and toxicity prediction were predicted.

2. Results and discussion

2.1. Chemistry

The synthetic pathways for synthesis pyridine and 1,2,4-triazine derivatives were illustrated in Scheme 1 and 2 using 1,6-diamino-2-oxo-4-(thiophen-2-yl)-1,2-dihydropyridine-3,5-dicarbonitrile (**1a**) and 1,6-diamino-2-oxo-4-(furan-2-yl)-1,2-dihydropyridine-3,5-dicarbonitrile (**1b**) as starting materials. The 1,6-diamino-2-oxo-pyridine derivatives **1a** and **1b** were used as reactive intermediates due to their included two center of reaction, *N*-amino and *C*-amino centers, which may be able to react as mono or bi-nucleophile reagent to produce various heterocyclic molecules.[51–53] Our work was designed to form condensation reaction by synthetized new Schiff bases through treatment of 1,6-diamino-2-oxo-pyridine derivatives **1a,b** with different aldehydes through the *N*-amino center or condensation with di-ketones through *N*-amino and *C*-amino centers to afford polycyclic compounds containing pyridine in its core. Moreover, to keep pace with the development in the preparation of organic materials, the condensation reaction takes place with conventional method and green chemistry method using a clean and rapid ceric ammonium nitrate CAN-catalyst instead of hazardous catalysts, such as acetic acid. The advantage of the reaction in the case of using CAN as a catalyst is that the reaction has occurred by stirring at room temperature for a short time and with good yield compared to the other hazardous methods.[54–56]

Treatment of 1,6-diamino-2-oxo-pyridine derivatives **1a,b** with different aldehydes such as 4-ethoxybenzaldehyde, 5-bromo-2-hydroxybenzaldehyde, 2-hydroxynaphthaldehyde, and 9-anthraldehyde in either refluxing solution in the presence of acid catalyst (acetic acid) or stirring the solution in the presence of cerium ammonium nitrate at room temperature to produce the corresponding Schiff base derivatives **2a,b**, **3a,b**, **4a,b**, and **5a,b**, respectively (Scheme 1). The structures of Schiff base

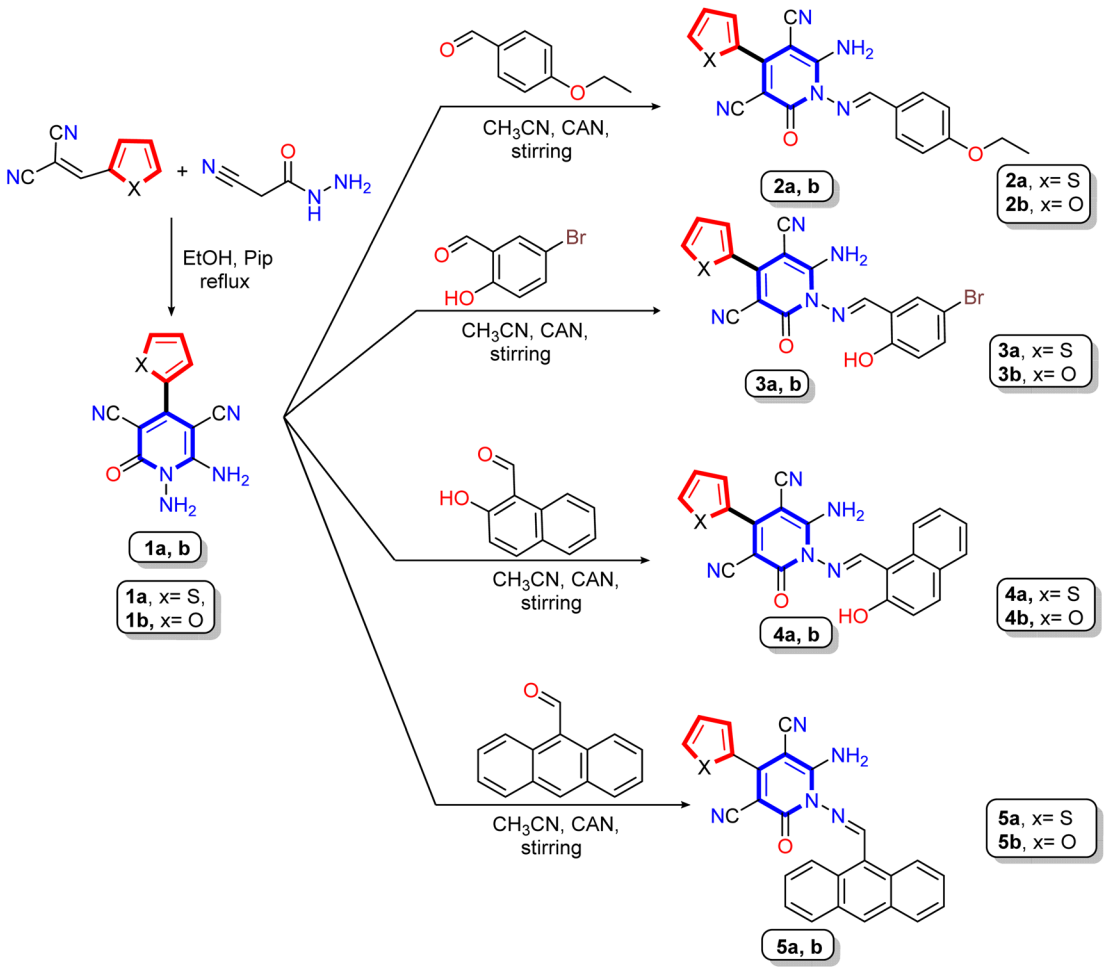

Scheme 1 Synthetic pathway for reaction of the starting materials 1,6-diamino-2-oxo-pyridine derivatives **1a,b** with different aldehydes.

derivatives were confirmed using elemental (CHN) and spectral analysis (IR, ^{1}H NMR, and ^{13}C NMR). Thus, the IR spectrum of compounds **2a,b**, as an example, showed absorption bands between ν 3438 to 3300 cm^{-1} for amino groups and cyano group at ν 2214 and 2213 cm^{-1}, as well as bands for carbonyl group between ν 1670–1668 cm^{-1}, and Schiff base imine group (C=N) at ν 1628 and 1627 cm^{-1}, respectively. Additionally, the ^{1}H NMR spectra of compound **2a** revealed two signals in the upfield region at δ 1.36 and 4.15 ppm as triplet and quartet referred to the ethoxy group, and the seven aromatic protons appeared as four doublets at δ 7.10, 7.45, 7.56, and 7.96 ppm and one triplet signals at δ 7.28 ppm. As well, a broad singlet signal appeared at δ 8.46 ppm assignable to two amino protons (NH_2), besides the methine protons (–CH=N–) at δ 8.79 ppm. The ^{13}C NMR spectrum of compound **2b** displayed specific signals at δ 14.99 and 64.11 ppm attributed to the ethoxy, signals at δ 84.04, 159.64, 163.06, 164.07, and 172.21 ppm related to carbon linked to the cyano group, methine carbon (–CH=N–), carbon linked attached to the amino group and ethoxy group, and carbonyl group (C=O), respectively.

By the same manner, the IR spectrum of compound **4a,b** revealed absorption bands between 3393 and 3315 cm^{-1} assigned to amino (–NH_2) and hydroxyl groups (–OH), as well as the cyano group bands appear at ν 2213 and 2207 cm^{-1}, besides two bands related to carbonyl group (C=O) and methine-CH (–CH=N–) displayed in the range of ν 1655–1640 cm^{-1} and 1631–1599 cm^{-1}, respectively. The ^{1}H NMR spectra of compound **4a** exhibited three specific singlet signals at δ = 8.47, 9.09 and 10.94 ppm assigned to amino protons (–NH_2), methine-CH, and hydroxyl proton (–OH), respectively. In addition to nine aromatic protons between δ 7.29–8.25 ppm as five doublet and one triplet. Moreover, the ^{13}C NMR spectrum of Schiff base **4a** assigned three singlet signals at δ 155.07, 157.55, and 164.92 ppm due to carbon linked to amino, hydroxyl groups, and carbonyl carbons, respectively. In addition, four significant signals at δ 84.28, 116.34, 116.94, and 154.02 related to carbon attached to cyano group, two nitrile functions, and methine-carbon (C=N) respectively, as well as the aromatic carbons ranged from δ 113.50 to 146.84 ppm.

Furthermore, our work extended to the synthesis of poly-cyclic compounds; the starting materials **1a,b** was subjected to react with cyclic-ketone containing poly carbonyl groups as ninhydrin and or/isatin to produce the isolable intermediate Schiff base derivatives **6a,b** and **8a,b**, respectively (Scheme 2). The elemental and spectral data confirmed the structure of the prepared compounds. The ^{1}H NMR of Schiff base derivative **8a**

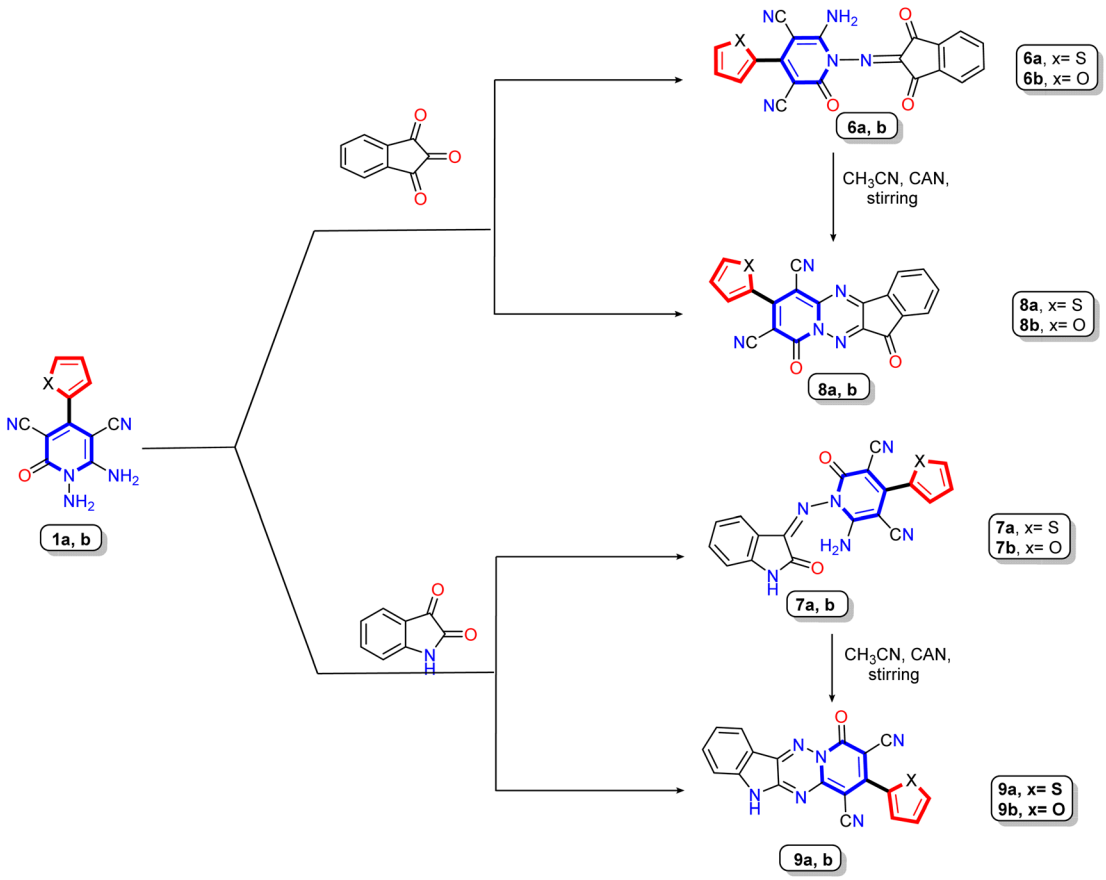

Scheme 2 Synthesis of Schiff's base derivatives **6a,b** and **8a,b** and their cyclization to produce tetracyclic compounds **7a,b** and **9a,b**.

showed two significant singlet signals at δ 8.4 and 11.02 ppm due to amino protons (NH_2) and –NH proton of the isatin molecule, besides the seven aromatic protons ranging from δ 6.78 to 7.56 ppm, where the thiophene protons appear as one doublet at δ 7.33 ppm with coupling constant $J = 3.6$ Hz and two doublet signals at δ 6.78 and 6.89 ppm with coupling constant J = 4.9 and 3.2 Hz, respectively. The four aromatic protons related to the isatin nucleus displayed as two doublets at δ 7.06 and 7.48 ppm with coupling constant J = 7.2 Hz and one doublet signal with integration two at 7.56 ppm. The ^{13}C NMR spectrum of the same compound revealed characteristic signals at δ 109.15, 114.10, 155.08, 166.09, and 172.12 ppm due to two cyano groups, imino carbon (C=N), and two carbonyl carbons, respectively.

In medicinal chemistry, polycyclic ring structures or fused rings serve as useful building blocks for developing multifunctional drugs and improving pharmacokinetics.[57,58] The target tetracyclic compounds **7a,b** and **9a,b** were synthesized by the reaction of 1,6-diamino-pyridine derivatives **1a,b** as binucleophile with bi-electrophile molecules (ninhydrin and isatin) and therefore occurred condensation reaction. The structure of polycyclic compounds **7a,b** and **9a,b** was confirmed chemically by heating or stirring of Schiff base derivatives **6a,b** and **8a,b** in the presence of specific catalyst (acid or CAN) to produce the target polycyclic compounds **7a,b** and **9a,b** *via* cyclization reaction (Scheme 2). For more details, the target polycyclic compounds were prepared using four different methods (see Experimental section). Compared to the conventional methods, the best yield was obtained when using cerium ammonium nitrate as a green catalyst at room temperature. Elemental and spectral data confirmed the structure of compounds. The IR spectrum of **7a,b** displayed stretching absorption bands due to two carbonyl and cyano groups at the exact frequencies. Also, ^{1}H NMR of spectrum of compound **7a** showed seven aromatic protons ranging between δ 7.42–8.36 ppm classified as three protons for thiophene nucleus appear as doublet signal at δ 7.82 ppm with coupling constant J = 2.7 Hz and integration two and one triplet signal at δ 7.42 ppm with coupling constant $J = 4.3$ Hz and integration one, while the others four protons related to phenyl ring of indeneone core and appear as one multiplet and two doublet signals at δ 8.12–8.15, 8.20, and 8.36 ppm. The ^{1}H NMR of spectrum of compound **7b** displayed only signals for aromatic protons ranging between δ 7.25 to 8.21 ppm with three signals at δ 7.25, 7.51, and 7.80 ppm with coupling constant $J = 3.6$, 3.2, and 4.0 Hz corresponding to furan bioactive core. Moreover, the ^{13}C NMR of spectrum of compound **7a** assigned significant signals at δ 91.50 and 99.17 ppm due to two carbons attached to nitrile groups, two singlet signals at δ 114.68 and 115.67 ppm for two cyano groups, besides signals for imino carbon (–C=N)

and two carbonyl functions appeared at δ 156.20, 160.58, and 183.62 ppm, respectively. Similarly, the IR structure of compound **9a** revealed significant absorption bands at ν 3173, 2213, and 1647 cm^{-1} attributed to NH, nitrile (CN), and carbonyl functions, respectively. Moreover, the ^1H NMR spectra of the same compounds displayed one exchangeable singlet signal at δ 11.79 ppm for NH-isatin, besides seven aromatic protons ranging from δ 7.08 to 7.88 ppm. In addition, the ^{13}C NMR spectrum of compound **9a** revealed characteristic signals at δ 156.35, 163.69, and 168.83 ppm for two imino carbons (–C=N), and carbonyl group, respectively.

2.2. Antimicrobial evaluation

2.2.1. Antimicrobial activity of the synthesized compounds. The initial screening of antimicrobial activity was evaluated for all the newly designed pyridine derivatives using agar well diffusion assay. Gentamicin and Fluconazole were used as positive controls for antibacterial or antifungal activity, respectively. The results showed that most synthesized derivatives could halt microbial growth with different percentages against tested pathogens. The antimicrobial activity of the tested derivatives is displayed in Tables 1 and S1† that represented by millimeters (mm). The pyridine derivatives **2–9** showed moderate to good antimicrobial activity.

For methicillin-sensitive *Staphylococcus aureus* (MSSA) as a Gram-positive bacterial, the pyridine derivatives **2**, **6**, **7**, and **8** that included thiophene moiety in position four displayed inhibition zones ranging from 18.3 ± 0.57 mm to 20.3 ± 0.57 mm higher than their analog furan-pyridine derivatives. In contrast, the combination of furan with pyridine showed higher activity in the case of compounds **3**, **4**, **5**, and **9**, with a zone of inhibition ranging from 17.3 ± 0.57 mm to 23.3 ± 0.57 mm compared with thiophene-pyridine derivatives and Gentamicin as a positive control (IZ = 19.6 ± 0.57 mm). The most active compounds against MSSA strain were revealed by furan–pyridine derivative **3b** by IZ = 23.3 ± 0.57 mm. Additionally, for methicillin-resistant *Staphylococcus aureus* (MRSA), the synthesized pyridine derivatives **2–9** showed zone of inhibition ranging from 13.3 ± 0.57 mm to 20.3 ± 0.57 mm in comparison to Gentamicin (IZ = 22.3 ± 0.57 mm). The highest activity of 2-oxo-4-(thiophen-2-yl)-1,2-dihydropyridine derivative **3b** against MSSA and MRSA may be attributed to the presence of the hydroxy group in position two and bromo atom in position five in the benzylidene ring at N_1 of 1,6-diaminopyridine motif. Moreover, replacing the bromo atom with a fused phenyl ring to form N_1-(2-hydroxynaphthalene)pyridine derivatives **4a,b** don't enhance the activity indicating that the bromo atom has an important effect on antibacterial activity.

For Gram-negative strains from family of Enterobacteriaceae, all the designed pyridine derivatives **2**, **3**, **4**, **5**, **6**, and **8** and tetracyclic derivatives **7** and **9** revealed higher activity against *Klebsiella pneumoniae* with zone of inhibition ranging from 18.3 ± 0.57 mm to 25.3 ± 0.57 mm compared to Gentamicin as a positive control (IZ = 18.3 ± 0.57 mm). Moreover, for

Table 1 The inhibition zone diameters mean ± SD expressed by (mm) of all synthesized derivatives **2a–9b** against different pathogenic microorganisms[a]

	Bacteria						
			Gram −ve				
	Gram +ve		Enterobacteriaceae		Non-Enterobacteriaceae		Fungi
Cpd no.	MSSA	MRSA	*E. coli*	*K. pneumoniae*	*P. aeruginosa*	*A. baumannii*	*C. albicans*
2a	18.3 ± 0.57	13.4 ± 0.57	13.3 ± 0.57	25.3 ± 0.57	18.3 ± 0.57	22.3 ± 0.57	16.3 ± 0.57
2b	16.3 ± 0.57	13.3 ± 0.57	17.3 ± 0.57	21.3 ± 0.57	18.3 ± 0.57	22.6 ± 0.57	18.3 ± 0.57
3a	20.3 ± 0.57	15.3 ± 0.57	15.3 ± 0.57	20.3 ± 0.57	20.3 ± 0.57	20.3 ± 0.57	16.3 ± 0.57
3b	23.3 ± 0.57	20.3 ± 0.57	16.7 ± 0.57	20.3 ± 0.57	18.3 ± 0.57	21 ± 1.00	14.3 ± 0.57
4a	15.3 ± 0.57	15.3 ± 0.57	17.3 ± 0.57	20.3 ± 0.57	18.3 ± 0.57	23.3 ± 0.57	16.6 ± 0.57
4b	20.3 ± 0.57	16.3 ± 0.57	17.6 ± 0.57	20.3 ± 0.57	15.3 ± 0.57	20.3 ± 0.57	13 ± 1.00
5a	18.3 ± 0.57	14.3 ± 0.57	17.3 ± 0.57	20.3 ± 0.57	15.3 ± 0.57	21 ± 1.00	15.3 ± 0.57
5b	18.3 ± 0.57	16.3 ± 0.57	16.6 ± 0.57	22.3 ± 0.57	16.3 ± 0.57	21 ± 1.00	15.3 ± 0.57
6a	18.3 ± 0.57	18.3 ± 0.57	17.3 ± 0.57	20.3 ± 0.57	17.3 ± 0.57	30.3 ± 0.57	15.3 ± 0.57
6b	17.3 ± 0.57	16.3 ± 0.57	18.3 ± 0.57	20.3 ± 0.57	18.3 ± 0.57	16 ± 1.00	15.6 ± 0.57
7a	20.3 ± 0.57	17.3 ± 0.57	14.6 ± 0.57	19 ± 1.00	12.3 ± 0.57	26.3 ± 0.57	15.3 ± 0.57
7b	15.3 ± 0.57	—	15.3 ± 0.57	20.3 ± 0.57	16 ± 1.00	25.3 ± 0.57	13 ± 1.00
8a	20.3 ± 0.57	15.3 ± 0.57	15.3 ± 0.57	18.3 ± 0.57	15.3 ± 0.57	23.3 ± 0.57	15.3 ± 0.57
8b	13.3 ± 0.57	14.3 ± 0.57	16.6 ± 0.57	22 ± 1.00	16.3 ± 0.57	23.3 ± 0.57	14.3 ± 0.57
9a	16 ± 1.00	15.3 ± 0.57	15.3 ± 0.57	19 ± 1.00	15 ± 1.00	23.3 ± 0.57	12.3 ± 0.57
9b	17.3 ± 0.57	15.3 ± 0.57	14.6 ± 0.57	18.3 ± 0.57	20.3 ± 0.57	18.3 ± 0.57	15.3 ± 0.57
Gen.	19.6 ± 0.57	22.3 ± 0.57	18.3 ± 1.52	18.3 ± 0.57	17.3 ± 0.57	22 ± 1.00	NA
FCZ	NA	NA	NA	NA	NA	NA	16.3 ± 1.15

[a] Well diameter = 8 mm, MSSA = methicillin sensitive *S. aureus* (ATCC 25923), MRSA = methicillin resistant *S. aureus* (ATCC 43300); *Escherichia coli* = *E. coli* (ATCC-25922) and *K. pneumoniae* = *Klebsiella pneumoniae* (ATCC-700603); *P. aeruginosa* = *Pseudomonas aeruginosa* (ATCC-2785), and *A. baumannii* = *Acinetobacter baumannii* (ATCC-19606); *C. albicans* = *Candida albicans* (ATCC-10231) Gen. = Gentamicin; FCZ = Fluconazole.

Klebsiella pneumoniae the 1-((4-ethoxybenzylidene)amino)-2-oxo-4-(thiophen-2-yl)-pyridine derivative **2a** showed the highest width for zone of inhibition (IZ = 25.3 ± 0.57 mm) and that may be due to the presence of ethoxy group attached to benzylidene at N_1 that donating electron to N_1 and therefore to pyridine nucleus. In addition, for *Escherichia coli* strain, the 6-amino-1-((1,3-dioxo-1,3-dihydro-2*H*-inden-2-ylidene)amino)-4-(furan-2-yl)-2-oxo-pyridine derivative **6b** and 6-amino-4-(furan-2-yl)-1-(((2-hydroxynaphthalen-1-yl)methylene)amino)-2-oxo-pyridine derivative **4b** displayed the most active members among these group with zone of inhibition (IZ = 18.3 ± 0.57 and 17.6 ± 0.57 mm), respectively, and compared with Gentamicin (IZ = 18.3 ± 1.52 mm). In contrast, the other derivatives exhibited very close zone of inhibition (13.3 ± 0.57 to 17.3 ± 0.57 mm).

For other Gram-negative strains outside family of Enterobacteriaceae (including, *Pseudomonas aeruginosa* and *Acinetobacter baumannii*) the tested pyridines and tetracyclic-containing pyridines appeared to effective with good diameter for zone of inhibitions indicating a broad-spectrum activity. Surprisingly, most of the pyridine derivatives exhibited super activity with a higher zone of inhibitions against non-Enterobacteriaceae strains compared with Gentamicin. The designed pyridine derivatives **2**, **3**, **4**, **5**, **6**, and **8** exhibited zone of inhibitions (IZ) ranging between (15.3 ± 0.57 to 20.3 ± 0.57 mm) and (16 ± 1.00 to 30.3 ± 0.57 mm) compared with Gentamicin (IZ = 17.3 ± 0.57 and 22 ± 1.00 mm) against *P. aeruginosa* and *A. baumannii* strains, respectively. Additionally, the 9-(furan-2-yl)-7-oxo-[1,2,4]triazino[5,6-*b*]indole derivative **9b** and 6-amino-1-((5-bromo-2-hydroxybenzylidene)-amino)-2-oxo-4-(thiophen-2-yl)-pyridine derivative **3a** displayed equipotent activity with the highest zone of inhibition (IZ = 20.3 ± 0.57 mm) against to *P. aeruginosa* and higher than Gentamicin (IZ = 17.3 ± 0.57 mm), as well as higher than other tetracyclic derivatives **7a**, **7b**, and **9a** that showed IZ = 12.3 ± 0.57, 16 ± 1.00, and 15 ± 1.00 mm, respectively. On the other hand, the 9-(furan-2-yl)-7-oxo-[1,2,4]triazino[5,6-*b*]indole derivative **9b** revealed the lowest activity against *A. baumannii* with the zone of inhibitions (IZ = 18.3 ± 0.57 mm) compared with others tetracyclic derivatives **7a**, **7b**, and **9a** that showed IZ = 26.3 ± 0.57, 25.3 ± 0.57, 23.3 ± 0.57 mm, respectively and compared with the Gentamicin (IZ = 23.3 ± 0.57 mm). For antifungal activity (*Candida albicans*), four derivatives **2a**, **2b**, **3a**, and **4a** among the sixteen derivatives that synthesized displayed zone of inhibition IZ = 16.3 ± 0.57, 18.3 ± 0.57, 16.3 ± 0.57 and 16.6 ± 0.57 mm higher than Fluconazole (IZ = 16.3 ± 1.15 mm). In addition, the rest of the other derivatives showed good antifungal activity with a zone of inhibitions ranging between 12.3 ± 0.57–15.6 ± 0.57 mm.

Finally, it can be concluded that the designed pyridine or tetracyclic containing pyridine derivatives with furan or thiophene moiety exhibited good to moderate activity against bacteria strains and yeast (*Candida albicans*). In addition, the conversion of the amino group at N_1 to imino group (C=N) conjugated with benzylidene moiety or 1,3-dioxo-1,3-dihydro-2*H*-inden-2-ylidene derivatives showed broad spectrum among all the tested strains with a zone of inhibition in most cases higher than Gentamicin and Fluconazole as positive antibiotic controls compared with 2-hydroxynaphthalen-1-ylene, anthracen-9-ylmethylene, and tetracyclic derivatives. Moreover, the designed derivatives' activity increases by increasing the number of oxygen atoms attached to the arylidine-imino group attached to N_1 of 1,6-diamino-2-oxo-pyridine derivatives.

2.2.2. Minimum inhibitory concentration (MIC) for most active derivatives. Following the first screening by agar diffusion method, the most active compounds **2a**, **2b**, **3a**, **3b**, **6a**, and **6b** were further tested to determine the minimum inhibitory concentrations by broth microdilution method. The results showed that the most active synthesized compounds demonstrated variable activities against different organisms. As illustrated in Table 2, for MRSA activity, the 6-amino-4-(furan-2-yl)-2-oxo-pyridine-3,5-dicarbonitrile derivatives **2b**, **3b**, and **4b** demonstrated two folds higher potency with inhibitory activity (MIC = 125, 62.5, and 125 μg mL^{-1}) compared to their thiophene analogs **2a**, **3a**, and **6a**. Moreover, the pyridine derivatives **2b**, **3a**, **6b**, and Gentamicin showed equipotent activity against MRSA with MIC value of 125 μg mL^{-1}, while 2-oxo-pyridine derivative **3b** exhibited two folds higher than Gentamicin with MIC value of 62.5 μg mL^{-1}. In addition, introducing hydroxy and bromo

Table 2 Minimum inhibitory concentrations (μg mL^{-1}) of the most active pyridine derivatives

	Bacteria					
		Gram −ve				
	Gram +ve	Enterobacteriaceae		Non-Enterobacteriaceae		Fungi
Cpd no.	MRSA	*E. coli*	*K. pneumoniae*	*P. aeruginosa*	*A. baumannii*	*C. albicans*
2a	500	250	500	250	3.9	250
2b	125	125	15.6	250	3.9	250
3a	125	250	250	250	31.25	250
3b	62.5	250	250	250	125	250
6a	250	250	125	250	3.9	15.6
6b	125	250	125	62.5	15.6	250
Gen.	125	250	250	250	1.95	NA
FCZ	NA	NA	NA	NA	NA	62.5

groups to benzylidene causes enhancement of the inhibitory potency, as shown in pyridine derivatives **3a** and **3b** with MIC 62.5 and 125 μg mL^{-1}, which may be attributed to the nature of these groups. For non-Enterobacteriaceae Gram-negative bacteria, the designed pyridine derivatives **2a**, **2b**, and **6a** had the higher ability to inhibit *A. baumannii* stain with MIC values 3.9 μg mL^{-1} followed by pyridine derivative **6b** (MIC = 15.6 μg mL^{-1}), **3a** (MIC = 31.25 μg mL^{-1}), and **3b** (MIC = 125 μg mL^{-1}), compared to Gentamicin (MIC = 1.95 μg mL^{-1}). Furthermore, for *P. aeruginosa*, the 1-((1,3-dioxo-1,3-dihydro-2*H*-inden-2-ylidene)amino)pyridine derivative **6b** that presented MIC = 62.5 μg mL^{-1} exhibited four folds higher than other derivatives **2a**, **2b**, **3a**, **3b**, **6a**, and Gentamicin (MIC = 250 μg mL^{-1}).

Furthermore, we further evaluated the MIC values for the most active derivatives against Enterobacteriaceae strains (*E. coli* and *K. pneumoniae*). The 1-((4-ethoxybenzylidene)amino)-2-oxo-4-(furan-2-yl)-pyridine derivative **2b** represented MIC values 15.6 against *Klebsiella pneumoniae* with higher inhibitory activity with (MIC = 250–500 μg mL^{-1} and 16–32 folds) than the rest of pyridine derivatives and sixteen folds higher than Gentamicin (MIC = 250 μg mL^{-1}). In addition, for activity against *E. coli*, the pyridine derivatives **2a**, **3a**, **3b**, **6a**, and **6b** showed similar MIC 250 μg mL^{-1}, while compound **2b** displayed the lowest MIC 125 μg mL^{-1} and still demonstrated two-folds higher than Gentamicin (MIC = 250 μg mL^{-1}).

Regarding *Candida albicans*, all compounds showed a similar MIC of 250 μg mL^{-1}, except 2-oxo-pyridine derivative **6b**, which displayed the lowest MIC of 15.6 μg mL^{-1} by sixteen folds than other derivatives and four folds than Fluconazole (MIC = 62.5 μg mL^{-1}). Based on the above results, the 2-oxo-pyridine derivative **2b** had the best antimicrobial activity against three of the tested microorganisms (*A. baumannii*, *K. pneumoniae*, and *E. coli*) with the lowest MIC values of 3.9, 15.6, and 125 μg mL^{-1} compared to Gentamicin (MIC = 1.95, 250 and 250 μg mL^{-1}), respectively. At the same time, the pyridine derivative **6a** that containing 1,3-dioxo-1,3-dihydro-2*H*-inden-2-ylidene and thiophene pharmacophore exhibited the best inhibitory activity against *C. albicans* with MIC value 15.6 μg mL^{-1} compared to other derivatives (MIC = 250 μg mL^{-1}) and Fluconazole (MIC = 62.5 μg mL^{-1}).

2.2.3. Biocidal and biostatic activity. The minimum bactericidal/fungicidal concentrations were determined for the most active 2-oxo-pyridine derivatives and the ratio between MBC/MIC and MFC/MIC was calculated, where the activity was considered as bactericidal if MBC/MIC ≤ 4, and bacteriostatic if the ratio MBC or MFC/MIC > 4 as described previously.[59] As shown in Table 3, the most active derivatives **2a**, **2b**, **3a**, **3b**, **6a**, and **6b** displayed bactericidal and fungicidal properties with MBC = 1.95–250 μg mL^{-1} and MFC = 15.6–125 μg mL^{-1}.

Moreover, for *K. pneumoniae*, the 4-(furan-2-yl)-pyridine derivatives **2b** and **6b** exhibited MBC = 1.95 and 15.6 μg mL^{-1} higher than pyridine derivative **3b** (MBC = 31.25 μg mL^{-1}) and compared with Gentamicin (MBC = 62.5 μg mL^{-1}). Similarly, the 4-(furan-2-yl)-pyridine derivatives **3b** and **6b** demonstrated MBC = 15.6 μg mL^{-1} compared to Gentamicin MBC = 31.25 μg mL^{-1} against MRSA strain. Moreover, compound **6b** demonstrated slightly bactericidal resistance on *P. aeruginosa* with MBC value of 31.25 μg mL^{-1} with two folds higher than Gentamicin (MBC = 62.5 μg mL^{-1}). Notably, for activity against yeast (*Candida albicans*), the 2-oxo-pyridine derivatives **2a**, **2b**, **3b**, and Fluconazole displayed equipotent MFC value of 62.5 μg mL^{-1}, while compound **6a** showed remarkable MFC value of 15.6 μg mL^{-1} with four folds higher than Fluconazole. In contrast, compounds **3a** and **6b** exhibited fungicidal potency with MFC value of 125 μg mL^{-1} nearly half of Fluconazole. As well, all pyridine derivatives had fungicidal potency based on ratio (0.25–0.50).

Table 3 Minimum bactericidal concentrations MBC (μg mL^{-1}) and minimum fungicidal concentration (MFC) (μg mL^{-1}) of the tested compounds and their ratio to MIC (MBC/MIC and MFC/MIC) represented by *R*[a]

	Bacteria											
	Gram +ve		Gram −ve								Fungi	
			Enterobacteriaceae				Non-Enterobacteriaceae					
	MRSA		*E. coli*		*Klebsiella pneumoniae*		*P. aeruginosa*		*A. baumannii*		*Candida albicans*	
Cpd no.	MBC	*R*	MBC	*R*	MBC	*R*	MBC	*R*	MBC	*R*	MFC	*R*
2a	125	<4	250	<4	125	<4	125	<4	1.95	<4	62.5	<4
2b	62.5	<4	125	<4	1.95	<4	125	<4	3.9	<4	62.5	<4
3a	62.5	<4	125	<4	250	<4	125	<4	7.8	<4	125	<4
3b	15.6	<4	125	<4	31.25	<4	250	<4	125	<4	62.5	<4
6a	250	<4	62.5	<4	125	<4	125	<4	1.95	<4	15.6	<4
6b	15.6	<4	125	<4	15.6	<4	31.25	<4	15.6	<4	125	<4
Gen.	31.25	<4	62.5	<4	62.5	<4	62.5	<4	1.95	<4	NA	NA
FCZ	NA	NA	NA	NA	NA	NA	NA	NA	NA	NA	62.5	1

[a] Gen. = Gentamicin; FCZ = Fluconazole.

Table 4 Percentage of inhibitory effect of 1/8 MIC of synthesized compounds on biofilm formation in various microorganisms[a]

	Biofilm inhibitory percentage (BI) at 1/8 MIC			
Cpd no.	MRSA	*E. coli*	*P. aeruginosa*	*C. albicans*
2a	27.6 ± 8.79	46.2 ± 0.95	1.6 ± 2.23	17.6 ± 0.92
2b	64.7 ± 1.85	63.2 ± 0.28	3.1 ± 2.41	29.7 ± 1.50
3a	61.5 ± 0.45	63.8 ± 0.45	0.70 ± 0.45	55.1 ± 2.77
3b	59.9 ± 2.60	43.0 ± 0.90	10.1 ± 3.32	20.7 ± 0.85
6a	55.5 ± 1.86	10.3 ± 2.36	26.5 ± 5.08	15.15 ± 5.26
6b	61.0 ± 0.90	63.8 ± 1.60	45.4 ± 1.30	75.0 ± 0.51
Gen.	52.3 ± 1.65	45 ± 0.45	29.4 ± 1.53	35.9 ± 2.51
Dox.	70.8 ± 0.45	68.3 ± 0.79	47.1 ± 1.48	—
Flu.	—	—	—	57.6 ± 1.7

[a] Gen. = Gentamicin; Dox. = Doxycycline; FCZ = Fluconazole.

Finally, the combination of pyridine with thiophene or furan at C4 and incorporation with benzylidene (containing electron donating group at ortho or para position) or 1,3-dioxo-1,3-dihydro-2*H*-indene moieties through imino group at N_1 of 1,6-diaminopyridine enhancement the bactericidal and fungicidal activity and in some cases exhibited super-activity compared to Gentamicin and Fluconazole.

2.2.4. Antibiofilm activity of the synthesized compounds. To examine the antibiofilm activity of the most active 2-oxo-pyridine derivatives **2a**, **2b**, **3a**, **3b**, **6a**, and **6b**, the microtiter plate method was applied against three bacterial strains (MRSA, *P. aeruginosa*, and *E. coli*), and one fungal pathogen (*C. albicans*), as examples that mostly produce biofilm. The percentage of biofilm inhibition (BI) were evaluated at 1/2, 1/4, and 1/8 MICs of the tested compounds and represented in Table S2† and biofilm inhibitory percentage at 1/8 MIC displayed in Table 4. The Gentamicin (Gen) and Doxycycline (Dox.) were used as positive controls.

For MRSA, the most active derivatives **6a** and **2b** exhibited good biofilm inhibition (BI) percentage values ranging from 55.5% to 64.7%, compared with Gentamicin (BI = 52.3 ± 1.65%) and Doxycycline (BI = 70.8 ± 0.45%), while compound **2a** showed lowest biofilm inhibitory percentage with value of 27.6%. Moreover, the biofilm inhibitory percentage of *E. coli* exhibited that compounds **2b**, **3a**, and **6b** represented biofilm inhibition nearly 63% higher than Gentamicin (BI = 45 ± 0.45%), but still near to Doxycycline (BI ~68.3%). In addition, 2-oxo-pyridine derivatives **2a** and **3b** demonstrated biofilm inhibitory percentage (BI ~46.2 and 43.0%) very close to Gentamicin (BI = 45 ± 0.45%). In contrast, compound **6a** showed the least biofilm inhibition of 10.3% against *E. coli*.

Regarding For *P. aeruginosa* biofilm activity, compound **6b** showed the highest percentage of biofilm inhibition with 45.4% and very close to Doxycycline (BI = 47.1%) and displayed 1.5 folds higher than Gentamicin (BI = 29.4%), followed by 2-oxo-pyridine derivatives **6a** and **3b** with biofilm inhibition percentages of nearly 26.5 and 10.1%, respectively. However, compounds **2a**, **2b**, and **3a** revealed a very low inhibition percentage (ranging from 0.7 to 3.1%). Moreover, the biofilm inhibitory percentage against *C. albicans* was tested. The results showed that 2-oxo-pyridines **6b** donated the highest percentage of biofilm inhibition of 75% compared with Fluconazole (BI = 57.6%). At the same time,

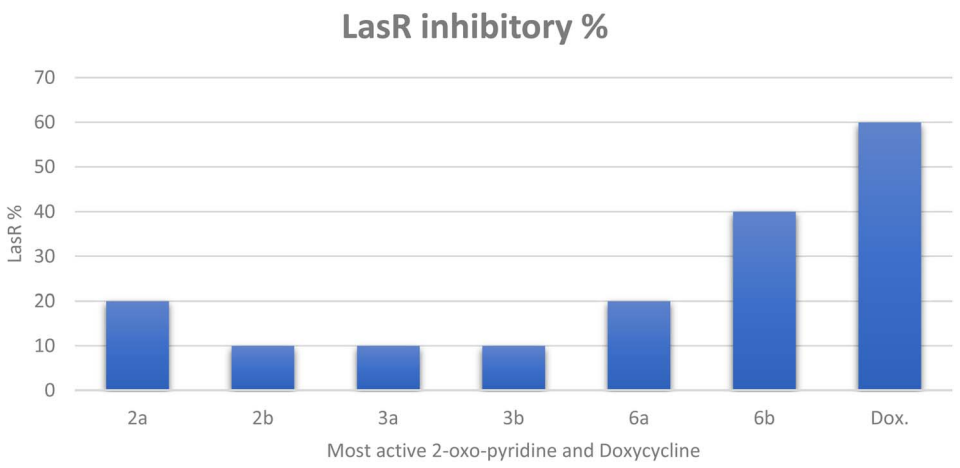

Fig. 2 The inhibitory percentage of *Las*R gene expression when treated with most active 2-oxo-pyridine derivatives **2a**, **2b**, **3a**, **3b**, **6a**, and **6b** at 1/8 MICs.

Table 5 The *in vitro* cytotoxic activity of the most active derivatives **2a**, **2b**, **3a**, **3b**, **6a**, and **6b** on Vero cell lines represented by μg mL^{-1}

Cpd no.	The *in vitro* cytotoxic activity of the most active derivatives on Vero cell lines ($IC_{50} \pm SD$) represented by μg mL^{-1}
2a	230.57 ± 6.52
2b	231.82 ± 2.21
3a	344.27 ± 3.81
3b	335.3 ± 7.95
6a	175.17 ± 3.49
6b	207.87 ± 5.14

compound **3a** revealed a biofilm inhibitory percentage of 55.1%, while compounds **2a**, **3b**, **2b**, and **6a** displayed a low biofilm inhibitory percentage (ranging from 15.15 to 29.7).

Finally, the most active derivatives showed good to potency biofilm inhibitory percentage at a low concentration from MIC value (1/8 MIC) compared to Gentamicin and Fluconazole. Moreover, compound **6b** exhibited the most active member by broad-spectrum against biofilm inhibitory percentage against the three bacterial strains (MRSA, *P. aeruginosa*, and *E. coli*), and *C. albicans* as a fungal pathogen. Additionally, compounds **2b** and **3a** revealed significant biofilm inhibition with values near Gentamicin against MRSA, and *E. coli*. The biofilm inhibitory percentage against *C. albicans* was tested, and the results showed that 2-oxo-pyridines **6b** and **3a** donated a high percentage of biofilm inhibition of 75 and 55.1%, respectively, while compounds **2a**, **3b**, **2b**, and **6a** displayed the lower percentage of biofilm inhibition (ranging from 15.15 to 29.7).

2.2.5. Effect of the synthesized compounds on the quorum sensing of *P. aeruginosa*. The *Las*R gene is a crucial gene that regulates QS in *P. aeruginosa* and is thought to act as a transcriptional activator of virulence genes in this serious bacterium. The effect of the most active synthesized 2-oxo-pyridines on the expression of the *Las*R gene at sub-MIC (1/8 MIC) was measured using quantitative real-time PCR. The results were calculated using the $2^{-\Delta\Delta Ct}$ using fluorescence real time PCR. Moreover, it was proved that Gentamicin couldn't affect the QS in *P. aeruginosa*.[60] Hence, Doxycycline was used as a positive control due to its reported anti-QS activity.[61] As represented in Table S3,† compound **6b** reduced the expression of the *Las*R gene by 40% compared to the bacteria not treated with synthesized compounds and Doxycycline (IB = 60%). A lower percentage was obtained by other synthesized compounds, where the *Las*R gene was reduced by 20% for compounds **2a**, **8a**, and 10% for compounds **3a**, **3b**, **2b** (Fig. 2).

Finally, it can be concluded that the most active derivatives could downstream the production of *Las*R-regulated virulence factors. Our findings regarding *P. aeruginosa*, the model microorganism for QS studies, suggest that these derivatives act as anti-virulence and anti-quorum sensing.

2.2.6. Cytotoxicity activity against normal cell line (Vero cells). One of the most important items in drug development is the evaluation of the toxicity of a new drug, where many clinical trials fail because of failures in toxicology evaluation, which is the crux of drug development.[62] Additionally, the effective drug exerts the desired physiological response without damaging normal cellular processes.[63,64]

The cytotoxic activity of the most active compounds on normal cell lines was evaluated to determine the safety of these derivatives. The IC_{50} values of the most active derivatives exhibited higher values ranging from 175.17 ± 3.49 to 344.27 ± 3.81 μg mL^{-1}, indicating that these derivatives exhibited anti-microbial activity without harmful effects on normal cellular structure and functions (non-toxic). The cytotoxicity of the synthesized compounds was evaluated using MTT assay[65,66] on

Table 6 Prediction of molecular properties, drug likeness and medicinal chemistry most active 2-oxo-pyridine derivatives **2a**, **2b**, **3a**, **3b**, **6a**, **6b**, and positive controls (Doxycycline and Gentamicin)[a]

		Most active 2-oxo-pyridine derivatives **2a**, **2b**, **3a**, **3b**, **6a**, **6b**, and positive controls (Doxycycline and Gentamicin)							
	Test items	**2a**	**2b**	**3a**	**3b**	**6a**	**6b**	DOX	Gen
SwissADME	**Molecular properties**								
	MLogP	1.64	0.85	1.80	1.01	0.31	−0.46	−2.08	−2.92
	TPSA (Å^2)	145.43	130.33	156.43	141.33	170.34	155.24	181.62	199.73
	M. wt.	389.43	373.36	440.27	424.21	399.38	383.32	444.43	477.60
	*n*HBA (NO)	5	6	5	6	6	7	9	12
	*n*HBD (OHNH)	1	1	2	2	1	1	6	8
	NRB	5	5	3	3	2	2	2	7
	Drug likeness and medicinal chemistry prediction								
	Log *S* (ESOL)	−4.07	−3.58	−4.54	−4.05	−3.86	−3.37	−2.59	0.24
	Solubility	M. soluble	Soluble	M. soluble	M. soluble	Soluble	Soluble	Soluble	H. soluble
	PAINS	0	0	1 (C=N)	1 (C=N)	0	0	0	0
	Lead-likeness	No (1)	No (1)	No (1)	No (1)	No (1)	No (1)	No (1)	No (1)
	Synthetic accessibility	3.36	3.46	3.27	3.36	3.53	3.62	5.15	6.51
	Bioavailability score	0.55	0.55	0.55	0.55	0.55	0.55	0.11	0.17
	Lipinski rule (violation)	Yes (0)	Yes (0)	Yes (0)	Yes (0)	Yes (0)	Yes (0)	Yes (1)	No (2)
	Veber rule (violation)	No (1)	Yes (0)	No (1)	No (1)	No (1)	No (1)	Yes (0)	No (1)

[a] M. soluble = moderately soluble; H. soluble = highly soluble; Dox. = Doxycycline; Gen. = Gentamicin.

Table 7 *In silico* toxicity prediction of most active 2-oxo-pyridine derivatives **2a**, **2b**, **3a**, **3b**, **6a**, **6b**, and positive controls (Doxycycline and Gentamicin)[a]

		Most active 2-oxo-pyridine derivatives **2a**, **2b**, **3a**, **3b**, **6a**, **6b**, and positive controls (Doxycycline and Gentamicin)							
Oral toxicity prediction		**2a**	**2b**	**3a**	**3b**	**6a**	**6b**	DOX	Gen
Oral toxicity prediction									
ProTox-II prediction	LD_{50} mg kg^{-1}	1000	1300	1000	600	600	600	1007	5000
	Toxicity class	IV	IV	IV	IV	IV	IV	IV	V
	Hepatotoxicity	Inactive	Inactive	Active	Active	Active	Active	Active	Inactive
		0.55	0.52	0.62	0.67	0.52	0.56	0.54	0.83
	Carcinogenicity	Active	Active	Active	Inactive	Active	Active	Inactive	Inactive
		0.55	0.57	0.50	0.50	0.58	0.60	0.77	0.74
	Immunotoxicity	Inactive	Inactive	Inactive	Inactive	Inactive	Inactive	Active	Active
		0.99	0.97	0.94	0.68	0.99	0.98	0.99	0.76
	Mutagenicity	Active	Inactive	Inactive	Inactive	Active	Active	Inactive	Inactive
		0.51	0.51	0.53	0.57	0.51	0.50	0.95	0.77
	Cytotoxicity	Inactive	Inactive	Inactive	Inactive	Inactive	Inactive	Inactive	Inactive
		0.86	0.84	0.67	0.73	0.88	0.89	0.90	0.66
	Heat shock factor response element (HSE)	Inactive	Inactive	Inactive	Inactive	Inactive	Inactive	Inactive	Inactive
		0.92	0.91	0.92	0.91	0.93	0.92	0.98	0.98
	Mitochondrial membrane potential (MMP)	Inactive	Inactive	Inactive	Inactive	Inactive	Inactive	Inactive	Inactive
		0.64	0.67	0.59	0.62	0.53	0.55	0.96	0.84
	Phosphoprotein (tumor suppressor) p53	Inactive	Inactive	Inactive	Inactive	Inactive	Inactive	Inactive	Inactive
		0.86	0.84	0.75	0.73	0.80	0.80	0.98	0.93

[a] DOX. = Doxycycline; Gen. = Gentamicin.

Vero cells (normal cell line) and the results revealed excellent findings of most active compounds **2a**, **2b**, **3a**, **3b**, **6a**, and **6b** with IC_{50} values of 230.57 ± 6.52, 231.82 ± 2.21, 344.27 ± 3.81, 335.3 ± 7.95, 175.17 ± 3.49, 207.87 ± 5.14 μg mL^{-1} respectively (Tables 5, S4 and Fig. S1†).

2.3. *In silico* studies

2.3.1. *In silico* drug-likeness properties and toxicity prediction. One of the most important methods in drug development is the quality of the designed compound and that is determined by its properties such as size, lipophilicity, shape, hydrogen bonding capability (donor and acceptors), and polarity of the molecules. As a result of their chemical and physical properties, chemical compounds exert their therapeutic effects on biomolecules in contact with them.[67,68] Our most active derivatives **2a**, **2b**, **3a**, **3b**, **6a**, and **6b** were evaluated to determine the molecular properties, drug likeness, and some medicinal chemistry prediction items as described in Table 6 compared with Doxycycline using SwissADME web tools as described previously.[69,70]

All the 2-oxo-pyridine derivatives exhibited obeys to Lipinski rule of five without any violation. Lipinski rule considered important predictors for drug candidate to be oral bioavailability with molecular weight (M. wt.) less than 500 dalton, number of hydrogen bond acceptors (NO) less than or equal ten, number of hydrogen bond donor (OHNH) less than or equal to five, and finally, the partition coefficient MLogP ≤ 4.15. In addition, the Doxycycline showed number of hydrogen donors = 6 (*i.e.*, higher than the standard rule), but belongs to Lipinski rule with one violation. On the other hand, Gentamicin doesn't fit the Lipinski rule due to two violations related to the number of hydrogen bond acceptors (*n*HBA (NO) = 12) and number of hydrogen bond donors (*n*HBD (OHNH) = 8). Moreover, all tested 2-oxo-pyridine derivatives **2a**, **3a**, **3b**, **6a**, **6b**, and Gentamicin don't fit to Veber rule due to their topological polar surface area TPSA > 140 Å, except furano-pyridine **2b** and Doxycycline Table 6.

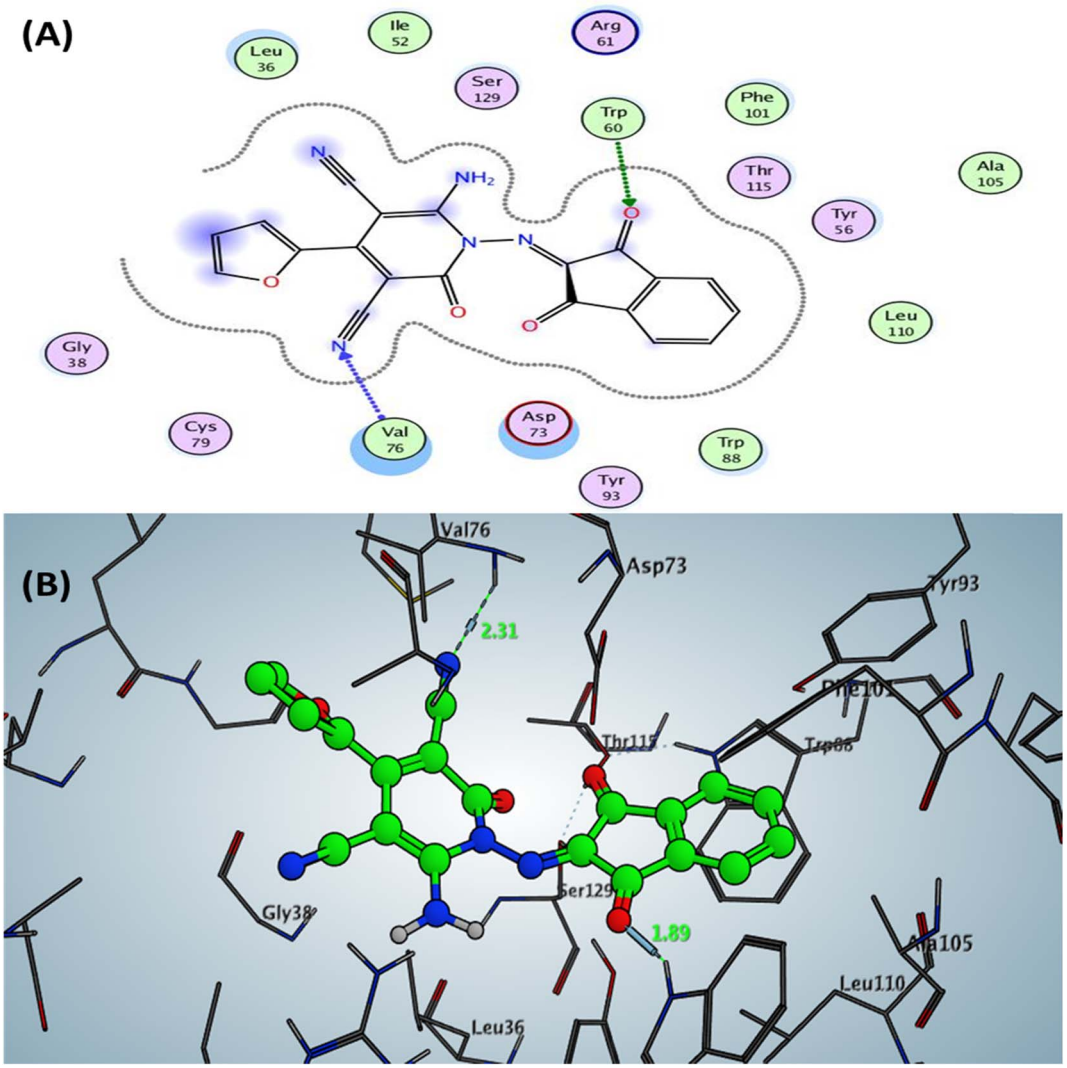

Fig. 3 Docking pose and ligand interaction of compound **6b** inside the active site of *Las*R (PDB: 6MVN) in *P. aeruginosa* (UCBPP-PA14) (A) 2D and (B) 3D structure.

Furthermore, in terms of drug likeness and medicinal chemistry predictions, three pyridine derivatives **2b**, **6a**, and **6b** demonstrated solubility properties with log *S* (ESOL) ranging from −0.46 to 0.85 compared to Doxycycline [log *S* (ESOL) = −2.08] and Gentamicin [log *S* (ESOL) = 0.24]. In addition, the rest of derivatives **2a**, **3a**, and **3b** exhibited moderate soluble with log *S* (ESOL) ranging from −4.54 to −4.05. Additionally, the values of synthetic accessibility indicated ease synthetic method with values ranging from 3.36 to 3.62 for most active derivatives compared with higher difficult synthetic accessibility to Doxycycline with values of 5.15 and Gentamicin (6.51). To our surprise, these derivatives exhibited an equal bioavailability score of 0.55, but still higher than positive controls. The drug likeness expression can be determined by how similar their properties are to those of existing drugs and all most active and positive controls (Doxycycline and Gentamicin) that showed violation in their molecular weight. The 6-amino-1-((5-bromo-2-hydroxybenzylidene)amino)-2-oxo-pyridine derivatives **3a** and **3b** showed the one Pan-assay interference compounds (PAINs) alarms due to imino group (C=N) in benzylidene moiety that has hydroxy group Table 6.

The *in silico* toxicity predictions were also conducted for the 2-oxo-pyridine derivatives to determine their adverse effects and toxicity using Protox-II web tool as the same method described previously[71,72] and the results listed in Table 7. The tested 2-oxo-pyridine derivatives belong to class four in toxicity classes according to globally harmonized system (GHS) that demonstrated LD_{50} from 600 mg kg^{-1} to 1300 mg kg^{-1} in comparison to Doxycycline (LD_{50} = 1007 mg kg^{-1}) and Gentamicin (LD_{50} = 5000 mg kg^{-1} that belongs to class V). The tested pyridine derivatives displayed non-cytotoxic and non-immunotoxin compared with Doxycycline and Gentamicin that displayed immunotoxin behavior with probability 0.99 and 76, respectively. In addition, all derivatives showed activity to carcinogenic with probability ranging from 0.50–0.60, except for compound **3b** and Doxycycline. For hepatotoxic, the 2-

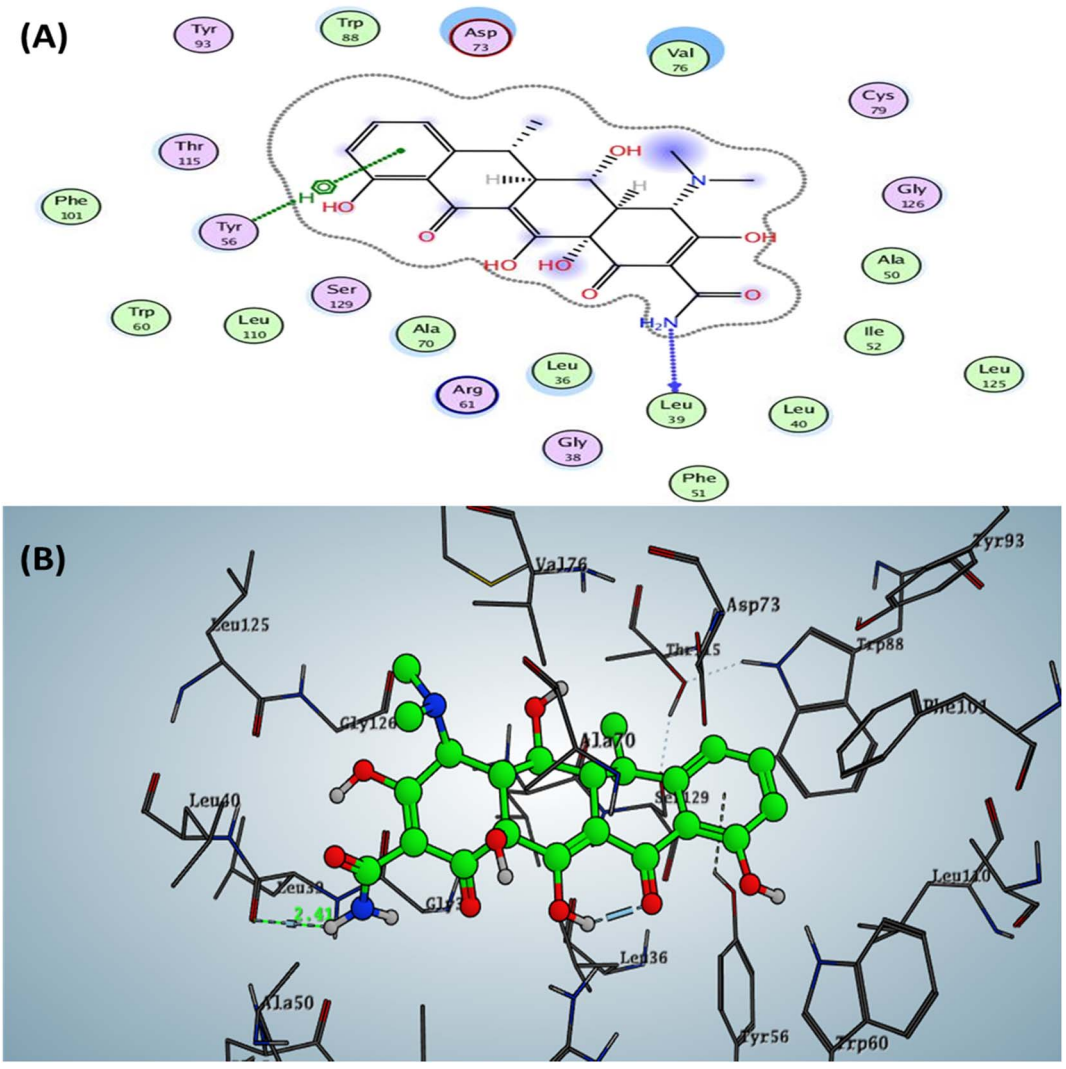

Fig. 4 Docking pose and ligand interaction of Doxycycline inside the active site of *Las*R (PDB: 6MVN) in *P. aeruginosa* (UCBPP-PA14) (A) 2D and (B) 3D structure.

oxopyridine expected to cause hepatotoxic, except 6-amino-1-((4-ethoxybenzylidene)amino)-2-oxo-pyridine derivative **2a** and **2b**, as well as Gentamicin. Additionally, three pyridine derivatives **2a**, **6a**, and **6b** increase rate of mutation, while the other derivatives **2b**, **3a**, **3b**, and positive controls (Doxycycline and Gentamicin) exhibited inactive mutagenic potential.

Finally, the most active derivatives revealed inactive to heat shock factor response, mitochondrial membrane potential, and phosphoprotein P53, *i.e.*, these compounds displayed a safety profile when administered as a candidate drug, and therefore, it can be further studied *in vivo* in the future.

2.3.2. Study binding interactions using docking simulation on LasR (PDB: 6MVN). A molecular docking simulation was carried out to analyze the interactions and binding modes of the most active 2-oxo-pyridine derivatives **2a**, **2b**, **3a**, **3b**, **6a**, **6b**, and Doxycycline as positive control inside the active site of the *Las*R. The docking process was performed using Molecular Operating Environment (MOE) software inside the active site of *Las*R protein (PDB: 6MVN) that was isolated from *P. aeruginosa* (UCBPP-PA14) with a resolution of 2.20 Å. The binding energy S = (kcal mol^{-1}) produced due to the complex formation between the docked compound and the protein's active site in the pocket. This energy involved many interactions, such as H-bond, electrostatic, and hydrophobic. Based on the *in vitro* results, compound **6b** exhibited the most active member among the tested derivatives with downregulation of the *Las*R gene with 40% compared with untreated *P. aeruginosa* (ATCC 2785). Compound **6b** displayed binding energy $S = -7.11$ kcal mol^{-1} with hydrogen bond sidechain acceptor between the residue Trp60 and oxygen of indane derivative at N_1 of pyridine with a bond length of 1.89 Å as the native co-crystallized ligand. Besides, one hydrogen bond backbone acceptor between the Val76 and nitrogen of the cyano group with a bond length of 2.31 Å Fig. 3. These two hydrogen bonds with hydrophobic

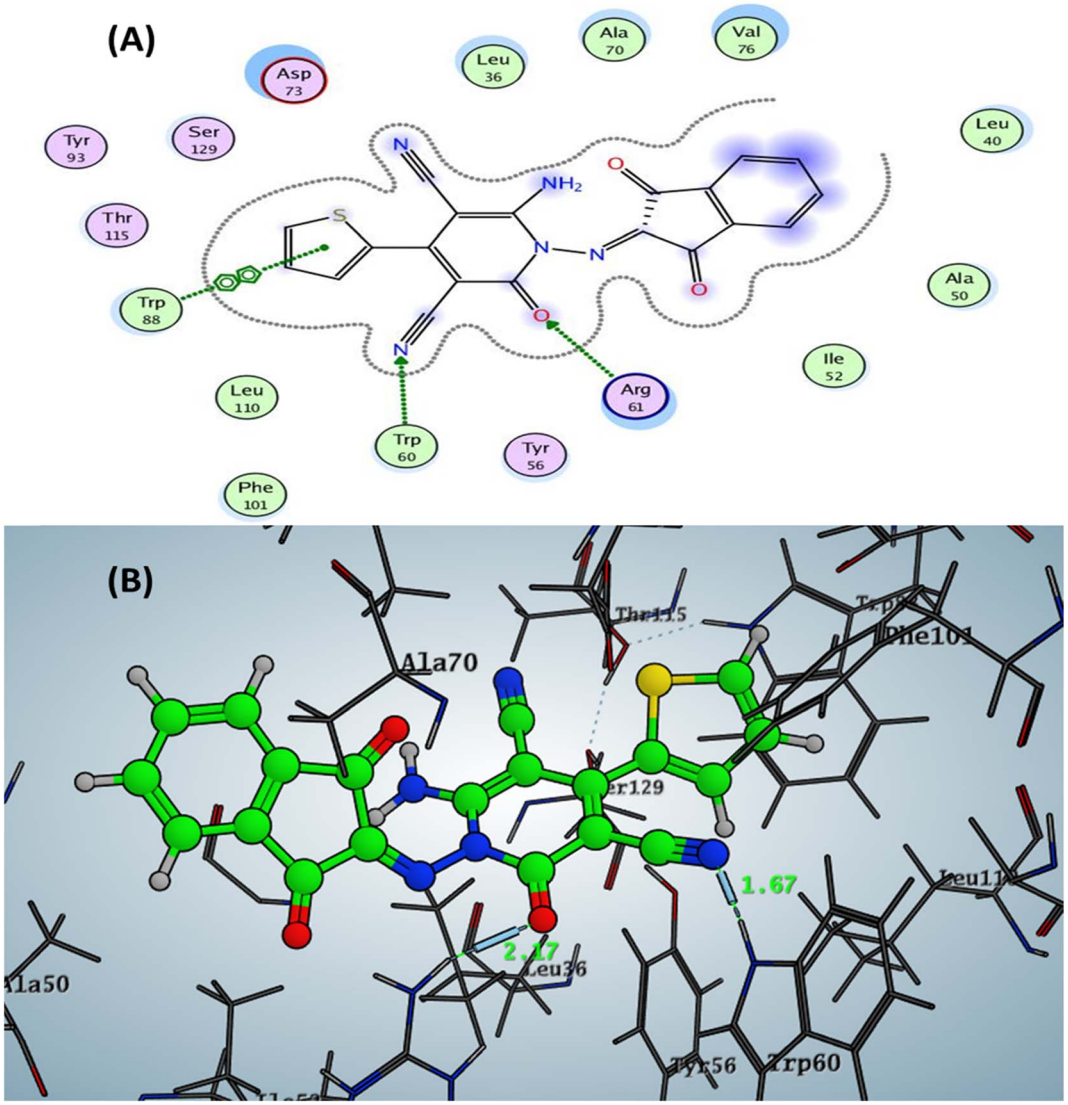

Fig. 5 Docking pose and ligand interaction of compound **6a** inside the active site of LasR (PDB: 6MVN) in *P. aeruginosa* (UCBPP-PA14) (A) 2D and (B) 3D structure.

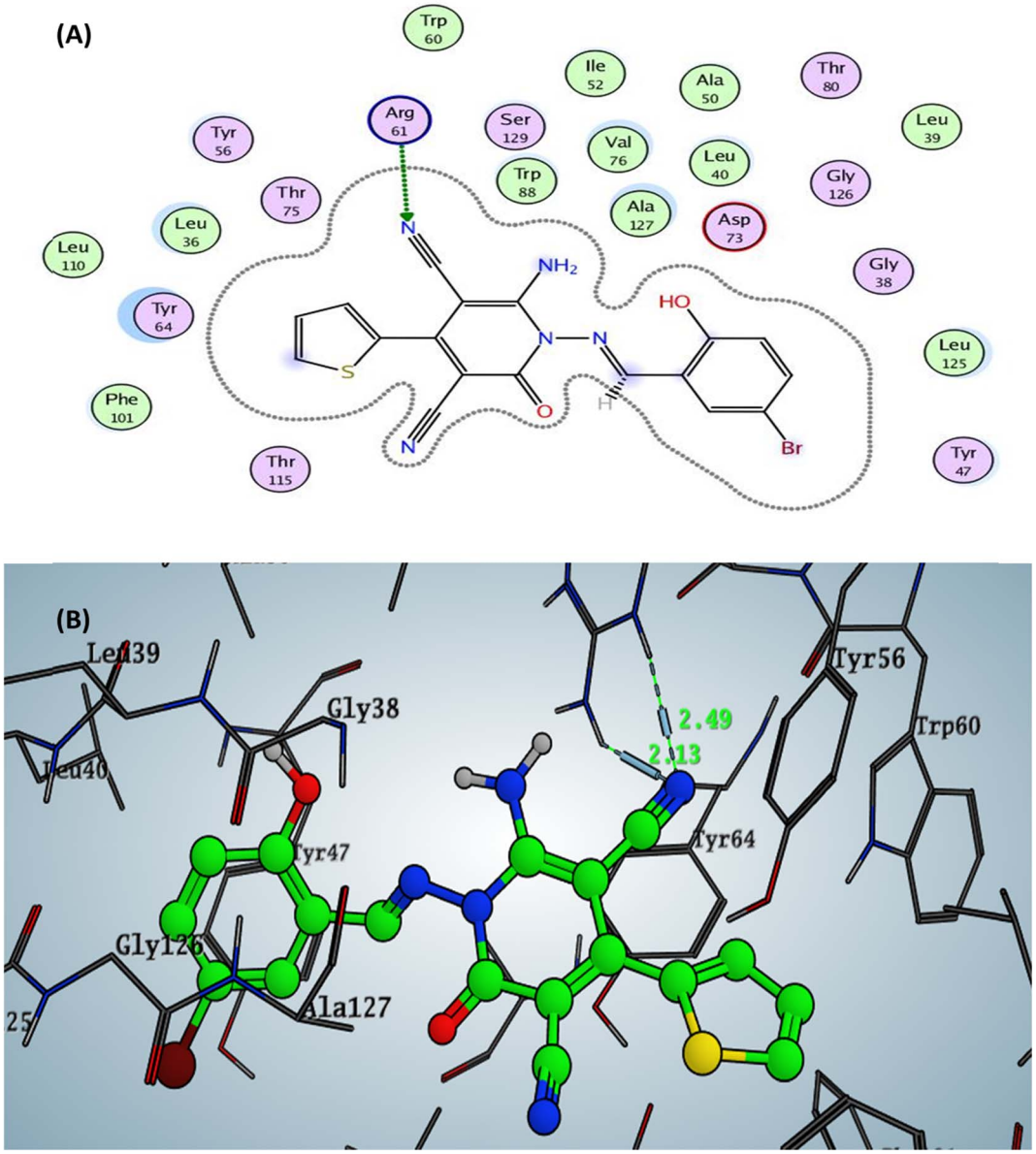

Fig. 6 Docking pose and ligand interaction of compound **3a** inside the active site of *Las*R (PDB: 6MVN) in *P. aeruginosa* (UCBPP-PA14) (A) 2D and (B) 3D structure.

interactions with the residue's amino acid, as represented in Fig. 3, might be explained the stabilization of the binding affinity with the target receptor and, therefore, may be responsible for its significant *in vitro* qPCR-*Las*R expression.

The Doxycycline as positive control revealed binding energy $S = -6.36$ kcal mol^{-1} (*in vitro* inhibitory percentage 60% at 1/8 MIC) with one backbone hydrogen bond donor between Leu39 and NH_2 of amide group at ring A in tetracyclic structure with a distance of 2.41 and arene–H interaction between phenyl of phenol at ring D with the amino acid Tyr56 Fig. 4. In contrast, compound **6a** demonstrated binding affinity $S = -7.02$ kcal mol^{-1} (*in vitro* inhibitory percentage 20% at 1/8 MIC) by forming two hydrogen bonds sidechain acceptors between the residue Arg61 and oxygen o carbonyl at C2 of pyridine nucleus and Trp60 with a nitrogen of nitrile group at C3 pf pyridine derivative with bond length 2.17 and 1.67 Å, respectively. In addition, Trp88 showed arene–arene interaction with the thiophene motif, as represented in Fig. 5.

The designed 4-thiophenyl-2-oxo-pyridine derivative **2a** and **3a** revealed binding energy $S = -6.74$ and -6.57 kcal mol^{-1} through hydrogen bond sidechain acceptor between the residue Arg61. Firstly, for compound **2a**, the arginine could form only one H-bond with the oxygen of the carbonyl group at C2 of the pyridine nucleus with a bond length of 2.45 Å. In contrast, compound **3a** displayed two hydrogen bonds with a nitrogen of nitrile group with a bond length of 2.13 Å (with NH_2 of arginine) and 2.49 Å (with nitrogen of imine of arginine). Moreover, the designed pyridine derivative **2b** exhibited binding energy $S = -6.51$ kcal mol^{-1} (*in vitro* inhibitory percentage 10% at 1/8 MIC) with two hydrogen bonds sidechain acceptors between Arg61

and oxygen of carbonyl at C2 and nitrogen of nitrile at C3 on the pyridine nucleus with bond lengths of 2.31 and 2.63 Å. In addition, the amino group at C6 of pyridine could form a hydrogen bond donor with the sidechain amino acid The75 with a bond length of 2.06 Å. The docking complex of compound **3b** demonstrated binding energy $S = -6.61$ kcal mol^{-1} (*in vitro* inhibitory percentage 10% at 1/8 MIC) through two hydrogen bonds with the sidechain residues. The first H-bond conducted between the Arg61 and the oxygen of carbonyl at C2 of pyridine with a bond length of 2.26 Å, while the other H-bond displayed with the hydroxyl group of benzylidene at N_1 of pyridine with a bond length 2.04 Å Fig. 6 (all figures with complete size represented in ESI file Fig. S2–S17†).

Finally, it can be concluded that the binding mode of furanone derivative and its binding energy as a co-crystallized ligand in the active site of the tested enzyme exhibited that our designed 2-oxo-pyridine nucleus act as QS inhibitors by downregulating *Las*R *via* H-bonds with the active site residues and hydrophobic interaction. Moreover, the carbonyl group at 2-oxo-pyridine derivative displayed H-bonds as the carbonyl of furanone.

3. Conclusion

This work introduced a new advancement in fighting *P. aeruginosa* by attenuating their virulence and disrupting their QS. A new series of 1,6-diamino-2-oxo-pyridine derivatives containing azomethine group at N_1 of pyridine containing different fragment pharmacophores or tetracyclic rings containing pyridine were synthesized by green chemistry using stirring and CAN as a catalyst and reflux approaches. The *in vitro* antimicrobial activity was screened for synthesized pyridine derivatives with six promising candidates. The most active compounds **2a**, **2b**, **3a**, **3b**, **6a**, and **6b** showed significant and broad spectrum with MIC values of 3.9–500 μg mL^{-1} against bacterial strains compared to Gentamicin (MIC = 1.95–250 μg mL^{-1}). Moreover, the MBC and MFC were determined, and their ratio with MIC revealed that these derivatives exhibited bactericidal and fungicidal potency. Anti-biofilm activity was evaluated against three bacteria (MRSA, *E. coli*, and *P. aeruginosa*) and *C. albicans* as fungal pathogen at concentrations 1/2, 1/4, and 1/8 MIC, and the results demonstrated strong reduction to biofilm formation. Furthermore, these six derivatives revealed down-regulation for the *Las*R gene as autoinducers for QS signals of *P. aeruginosa* with values ranging from 40 to 10% at low concentration (1/8 MIC) using the qPCR technique. The most active compound **6b** reduced the expression of the *las*R gene by 40% at 1/8 MIC compared to untreated *P. aeruginosa*. Subsequently, these derivatives exhibited IC_{50} values ranging from 175.17 ± 3.49 to 344.27 ± 3.81 μg mL^{-1} against Vero cells (normal cell lines), indicating non-toxic properties on normal cells. Additionally, the *in silico* ADMET properties, including molecular properties, drug-likeness, and some medicinal chemistry parameters, were predicted, and the tested pyridine derivatives possessed acceptable and good results as drug-like characteristics. The molecular docking simulation was determined for most active derivatives inside the *Las*R gene (PDB: 6MVN) to determine the binding mode interaction and binding energy that showed negative values ranging (−6.51 to −7.11 kcal mol^{-1}) and, therefore, suggested that these derivatives can be used for further *in vivo* studies. Finally, we concluded that these novel compounds could provide additive value in fighting *P. aeruginosa* by attenuating their virulence and QS to overcome the continuous emergence of resistant strains and encourage us to test the efficacy of these compounds on other bacterial strains in the future.

4. Experimental

4.1. Chemistry

4.1.1. Materials and instrumentation. All reagents and chemicals were ordered from Aldrich Chemicals without further purification, and solvents from Fisher. Melting points (MPs) of all the newly designed compounds were recorded on a digital Gallen Kamp MFB-595 instrument using open capillaries. Within the range of 400–4000 cm^{-1}, IR spectra were calculated using the KBr disc methodology on a Shimadzu 440 spectrophotometer. In NMR spectra (^{1}H/^{13}C), chemical shifts were calculated in δ ppm relative to TMS as an internal default (=0 ppm) that obtained on a JOEL spectrometer 400/100 MHz using DMSO-d_6 as solvents. The data was provided in the following format: chemical shift, multiplicity (br. = broad, m = multiplet, q = quartet, t = triplet, d = doublet, and s = singlet), coupling constant (J) in Hertz (Hz), and integration. Elemental analysis (within ±0.4% of the calculated value) was carried out at Cairo University's Micro Analytical Unit in Cairo. At Al-Azhar University's Regional Center for Biotechnology. The starting material 1,6-diamino-2-oxo-4-(thiophen-2-yl)-1,2-dihydropyridine-3,5-dicarbonitrile (**1a**) was prepared as orange powder and melting point 293–295 °C, reported according to the literature method.[73] Also, 1,6-diamino-2-oxo-4-(furan-2-yl)-1,2-dihydropyridine-3,5-dicarbonitrile (**1b**) was prepared as red powder and melting point 285–287 °C, reported according to the literature method.[73]

4.2. Synthesis of target compounds

4.2.1. General method for synthesis of target Schiff's base derivatives (2a,b, 6a,b and 7a,b)

4.2.1.1 Method (a). To a solution of pyridine derivatives **1a,b** (0.01 mmol) and the appropriate substituted aldehydes (0.01 mmol) or ketones (0.01 mmol) namely, 4-ethoxybenzaldehyde, 5-bromo-2-hydroxybenzaldehyde, 2-hydroxy-1-naphthaldehyde, and 9-anthraldehyde, ninhydrin, and isatin in dimethylformamide as a solvent catalyzed with acetic acid (1 mL). The solution mixture was heated under reflux for 3–6 h (monitoring by TLC). After the reaction is completed, the solution mixture was added to 20 mL cold ethanol, and the precipitated solid was filtered, washed with ethanol, dried, and crystallized from boiling with ethanol to yield the desired compounds.

4.2.1.2 Method (b). A mixture of pyridine derivatives **1a,b** (0.01 mmol), substituted aldehydes (0.01 mmol) or ketones (0.01 mmol) (4-ethoxybenzaldehyde, 5-bromo-2-hydroxybenzaldehyde, 2-hydroxy-1-naphthaldehyde, and

anthracene-9-carbaldehyde, ninhydrin, isatin), cerium ammonium nitrate (2 mol%) as Lewis acid catalyst, and acetonitrile (10 mL) as solvent were combined to a 100 mL rounded-flask and stirred at room temperature for 45–90 min (monitoring by TLC). After the reaction is completed, the solid product that precipitated was filtered out, washed with ethanol, dried, and crystallized from boiling with ethanol to produce the desired compounds with high yield.

*4.2.1.2.1 6-Amino-1-((4-ethoxybenzylidene)amino)-2-oxo-4-(thiophen-2-yl)-1,2-dihydro-pyridine-3,5-dicarbonitrile (**2a**).* M.p.: 215–217 °C; pale-yellow powder; yield 76% (89%); IR (KBr): ν_{max} 3425, 3301 (NH_2), 3080 (aromatic-H), 2981 (aliphatic-H), 2213 (CN), 1670 (CO), 1628 (CH = N); ^{1}H NMR (δ, ppm) 1.36 (t, 3H, $\underline{CH}_3CH_2O$), 4.15 (q, 2H, $CH_3\underline{CH}_2O$), 7.10 (d, J = 8.8 Hz, 2H, Ar–H), 7.28 (t, J = 4.8 Hz, 1H, thiophene-H), 7.45 (d, J = 8.8 Hz, 1H, Ar–H), 7.56 (d, J = 3.6 Hz, 1H, thiophene-H), 7.96 (d, J = 8.8 Hz, 2H, Ar–H), 8.46 (s, 2H, NH_2, D_2O exchangeable), 8.79 (s, 1H, methylinic-H); ^{13}CNMR (δ, ppm) 14.92 ($\underline{CH}_3CH_2O$), 64.11 ($CH_3\underline{CH}_2O$), 86.88 (<u>C</u>–CN), 115.34 (CN), 115.17 (CN), 116.07, 124.54, 128.22, 128.87, 129.96, 130.79, 131.25, 132.33, 132.45, 133.80, 152.12 (Ar–Cs), 157.24 (CH = N), 159.68 (C–NH_2), 164.02 (<u>C</u>–OEt), 172.45 (C=O); anal calcd. For $C_{20}H_{15}N_5O_2S$ (389.4): C, 61.68; H, 3.88; N, 17.98. Found: C, 67.61.52; H, 3.68; N, 17.81.

*4.2.1.2.2 6-Amino-1-((4-ethoxybenzylidene)amino)-2-oxo-4-(furan-2-yl)-1,2-dihydro-pyridine-3,5-dicarbonitrile (**2b**).* M.p.: 226–228 °C; pale-yellow powder; yield 77% (89%); IR (KBr): ν_{max} 3438, 3300 (NH_2), 3119 (aromatic-H), 2981 (aliphatic-H), 2214 (CN), 1668 (CO), 1627 (CH = N). ^{1}H NMR (δ, ppm) 1.35 (t, 3H, $\underline{CH}_3CH_2O$), 4.13 (q, 2H, CH3$\underline{CH}_2O$), 6.81 (d, J = 3.6 Hz, 2H, furan-H), 7.07 (t, J = 5.6 Hz, 1H, furan-H), 7.31 (d, J = 8.8 Hz, 1H, Ar–H), 7.82 (d, J = 8.8 Hz 1H, Ar–H), 7.94 (d, J = 8.8 Hz, 2H, Ar–H), 8.34 (s, 2H, NH_2, D_2O exchangeable), 8.75 (s, 1H, methylinic-H); ^{13}CNMR (δ, ppm) 14.99 ($\underline{CH}_3CH_2O$), 64.35 ($CH_3\underline{CH}_2O$), 84.04 (<u>C</u>–CN), 115.11, 115.28, (2CN), 116.26, 116.76, 117.58, 118.06, 124.35, 128.91, 130.02, 133.00, 145.22, 146.17, 147.51 (Ar–Cs), 159.64 (CH = N), 163.06 (C–NH_2), 164.07 (C–OEt), 172.21 (C=O); anal calcd. For $C_{20}H_{15}N_5O_3$ (373.37): C, 64.34; H, 4.05; N, 18.76. Found: C, 63.91.52; H, 3.98; N, 18.54.

*4.2.1.2.3 6-Amino-1-((5-bromo-2-hydroxybenzylidene)amino)-2-oxo-4-(thiophen-2-yl)-1,2-dihydropyridine-3,5-dicarbonitrile (**3a**).* M.p.: 288–290 °C; brown powder; yield 80% (91%); IR (KBr): ν_{max} 3305, 3210, 3102 (OH, NH_2), 2967 (aromatic-H), 2927 (aliphatic-H), 2215 (CN), 1654 (CO), 1621 (CH = N). ^{1}H NMR (δ, ppm) = 7.21 (t, 1H, thiophene-H), 7.31 (d, J = 3.0 Hz, 1H, thiophene-H), 7.34 (d, J = 7.1 Hz, 1H, Ar–H), 8.01 (d, J = 3.2 Hz, 1H, thiophene-H), 8.04 (d, J = 4.8 Hz, 1H, Ar–H), 8.07 (s, 1H, Ar–H), 8.33 (d, 2H, NH_2, D_2O exchangeable), 9.02 (s, 1H, methylinic-H), 10.56 (s, 1H, O–H, D_2O exchangeable); ^{13}CNMR (δ, ppm) 86.44 (<u>C</u>–CN), 113.08, 114.77, 115.64 (2CN), 116.26, 116.74, 118.35, 119.72, 127.97, 145.23, 145.68, 146.68, 146.82, 147.00 (Ar–Cs), 157.51 (CH = N), 157.66 (C–NH_2), 159.97 (C=O), 161.62 (C–OH); anal. calcd. For $C_{18}H_{10}BrN_5O_2S$ (440.28): C, 50.96; H, 2.38; N, 16.51. Found: C, 50.52; H, 2.26; N, 16.22.

*4.2.1.2.4 6-Amino-1-((5-bromo-2-hydroxybenzylidene)amino)-2-oxo-4-(furan-2-yl)-1,2-dihydro-pyridine-3,5-dicarbonitrile (**3b**).* M.p.: 246–248 °C; orange powder; yield 84% (90%); IR (KBr): ν_{max} 3295, 3201 (NH_2, OH), 2214 (CN), 1650 (CO), 1623 (CH = N). ^{1}H NMR (δ, ppm) 7.27 (t, J = 4.4 Hz, 1H, furan-H), 7.54 (d, J = 3.2 Hz, 1H, furan-H), 7.58 (d, J = 7.2 Hz, 1H, Ar–H), 7.62 (d, J = 3.2 Hz, 1H, furan-H), 7.93 (d, J = 6.8 Hz, 1H, Ar–H), 8.28 (s, 1H, Ar–H), 8.47 (s, 2H, NH_2, D_2O exchangeable), 9.05 (s, 1H, methylinic-H), 10.86 (s, 1H, OH, D_2O exchangeable); ^{13}CNMR (δ, ppm) 83.10 (<u>C</u>–CN), 115.28 (CN), 115.64 (CN), 116.74, 117.06, 120.01, 124.60, 132.32, 141.83, 145.14, 145.77, 146.05, 146.77, 146.98 (Ar–Cs), 157.74 (CH = N), 159.33 (C–NH_2), 159.90 (C=O), 161.52 (OH); anal. calcd. For $C_{18}H_{10}BrN_5O_3$ (424.21): C, 50.96; H, 2.38; N, 16.51. Found: C, 50.60; H, 2.26; N, 16.12.

*4.2.1.2.5 6-Amino-1-(((2-hydroxynaphthalen-1-yl)methylene)amino)-2-oxo-4-(thiophen-2-yl)-1,2-dihydropyridine-3,5-dicarbonitrile (**4a**).* M.p.: 388–390 °C; brown red powder; yield 65% (88%); IR (KBr): ν_{max} 3393, 3275, 3222 (NH_2, OH), 3054 (aromatic-H), 3018 (aliphatic-H), 2213 (CN), 1655 (CO), 1631 (CH = N); ^{1}H NMR (δ, ppm) 7.29 (t, J = 9.0 Hz, 1H, Ar–H), 7.57–7.64 (m, 4H, Ar–H), (d, J = 8.2 Hz, 2H, Ar–H), 7.94 (d, J = 8.0 Hz, 1H, Ar–H), 8.07 (d, J = 9.9 Hz, 2H, Ar–H), 8.25 (d, J = 9.6 Hz, 1H, Ar–H), 8.47 (d, 2H, NH_2, D_2O exchangeable), 9.09 (s, 1H, methylinic-H), 10.94 (s, 1H, OH, D_2O exchangeable); ^{13}CNMR (δ, ppm) 84.28 (<u>C</u>–CN), 113.50, 115.07, 116.34 (CN), 116.94 (CN), 117.20, 118.86, 119.61, 128.43, 128.68, 128.80, 129.96, 130.23, 139.14, 139.24, 145.11, 145.65, 146.84 (Ar–Cs), 154.02 (CH = N), 155.07 (C–NH_2), 157.55 (C–OH), 164.92 (C=O); anal. calcd. For $C_{22}H_{13}N_5O_2S$ (411.44): C, 64.22; H, 3.18; N, 17.02. Found: C, 63.88; H, 3.01; N, 16.78.

*4.2.1.2.6 6-Amino-4-(furan-2-yl)-1-(((2-hydroxynaphthalen-1-yl)methylene)amino)-2-oxo-1,2-dihydropyridine-3,5-dicarbonitrile (**4b**).* M.p.: 342–344 °C; gray powder; yield 67% (88%). IR (KBr): ν_{max} 3385, 3266, 3115 (NH_2, OH), 2926 (aliphatic-H), 2207 (CN), 1640 (CO), 1599 (CH = N); ^{1}H NMR (δ, ppm) 7.27 (t, J = 8.0 Hz, 1H, Ar–H), 7.58 (d, J = 3.2 Hz, 2H, furan-H), 7.95 (d, J = 4.3 Hz, 2H, furan-H), 8.02 (d, J = 8.1 Hz, 1H, Ar–H), 8.07 (d, J = 9.9 Hz, 2H, Ar–H), 8.25 (d, J = 8.4 Hz, 1H, Ar–H), 8.53 (d, 2H, NH_2, D_2O exchangeable), 9.09 (s, 1H, methylinic-H), 11.49 (s, 1H, OH, D_2O exchangeable). ^{13}CNMR (δ, ppm) 82.86 (<u>C</u>–CN), 113.96 (CN), 115.55 (CN), 116.32, 117.76, 118.86, 119.17, 119.87, 128.03, 128.53, 129.23, 129.63, 130.05, 139.11, 139.33, 145.03, 145.23, 146.69 (Ar–Cs), 153.84 (CH = N), 155.85 (C–NH_2), 157.43 (C–OH), 162.74 (C=O); anal. calcd. for $C_{22}H_{13}N_5O_3$ (395.38): C, 66.83; H, 3.31; N, 17.71. Found: C, 66.48; H, 3.11; N, 17.28.

*4.2.1.2.7 6-Amino-1-((anthracen-9-ylmethylene)amino)-2-oxo-4-(thiophen-2-yl)-1,2-dihydro-pyridine-3,5-dicarbonitrile (**5a**).* M.p.: 318–320 °C; brown powder; yield 73% (92%); IR (KBr): ν_{max} 3372, 3322 (NH_2), 3081 (aromatic-H), 2925 (aliphatic-H), 2212 (CN), 1691 (CO), 1647 (CH = N); ^{1}H NMR (δ, ppm) 7.24 (t, J = 3.6 Hz, 1H, thiophene-H), 7.51 (d, J = 2.8 Hz, 2H, thiophene-H), 7.68 (t, J = 7.6 Hz, 2H, Ar–H), 7.83 (t, J = 6.8 Hz, 2H, Ar–H), 7.90 (d, J = 5.6 Hz, 2H, Ar–H), 8.27 (d, J = 8.1 Hz, 2H, Ar–H), 8.78 (s, 2H, NH_2, D_2O exchangeable), 8.92 (s, 1H, Ar–H), 9.04 (s, 1H, methylinic-H); ^{13}CNMR (δ, ppm) 82.99 (<u>C</u>–CN), 116.26 (CN), 116.74, (CN), 117.47, 118.34, 118.57, 120.02, 121.21, 121.71, 124.60, 126.62, 130.38, 134.10, 134.46, 135.03, 135.98, 139.10,

145.23, 145.68, 146.78, 146.83, 147.51, 151.27 (Ar–Cs), 157.66 (CH = N), 161.64 (C–NH_2), 163.51(C=O); anal. calcd. For $C_{26}H_{15}N_5OS$ (445.50): C, 70.10; H, 3.39; N, 15.72. Found: C, 69.92; H, 3.38; N, 15.61.

*4.2.1.2.8 6-Amino-1-((anthracen-9-ylmethylene)amino)-4-(furan-2-yl)-2-oxo-1,2-dihydropyridine-3,5-dicarbonitrile (**5b**).* M.p.: 340–342 °C; brownish red powder; yield 69% (88%); IR (KBr): ν_{max} 3381, 3271 (NH_2), 3115 (aromatic-H), 2925 (aliphatic-H), 2206 (CN), 1670 (CO), 1640 (CH = N). ^{1}H NMR (δ, ppm) 6.81 (m, 2H, Ar–H), 6.86 (t, J = 4.0 Hz, 1H, furan-H), 7.33 (d, J = 3.6 Hz, 2H, furan-H), 7.63 (t, J = 7.2 Hz, 2H, Ar–H), 8.06 (d, J = 6.6 Hz, 2H, Ar–H), 8.21 (d, J = 8.0 Hz, 1H, Ar–H), 8.40 (s, 2H, NH_2, D_2O exchangeable), 8.78 (d, J = 8.8 Hz, 2H, Ar–H), 8.92 (s, 1H, methylinic-H); ^{13}CNMR (δ, ppm) 86.82 (C–CN), 114.80 (CN), 116.77 (CN), 116.92, 118.57, 120.15, 124.60, 127.83, 128.35, 129.79, 131.40, 135.70, 137.70, 138.84, 139.53, 142.01, 145.17, 145.35, 145.54, 146.07, 146.49, 146.91, 147.16 (Ar–Cs), 155.93 (C–NH_2), 157.60 (CH = N), 162.57 (C=O); anal. calcd. For $C_{26}H_{15}N_5O_2$ (429.43): C, 72.72; H, 3.52; N, 16.31. Found: C, 72.43; H, 3.30; N, 15.97.

*4.2.1.2.9 6-Amino-1-((1,3-dioxo-1,3-dihydro-2H-inden-2-ylidene)amino)-2-oxo-4-(thiophen-2-yl)-1,2-dihydropyridine-3,5-dicarbonitrile (**6a**).* M.p.: 281–283 °C; black powder; yield 73% (89%); IR (KBr): ν_{max} 3395, 3323 (NH_2), 3092 (aromatic-H), 2211 (CN), 1658 (2CO), 1582 (C=N); ^{1}H NMR (δ, ppm) 7.43 (t, J = 4.0 Hz, 1H, thiophene-H), 7.82 (d, J = 4.0 Hz, 1H, thiophene-H), 8.12 (t, J = 8.0 Hz, 2H, Ar–H), 8.25 (d, J = 8.0 Hz, 2H, Ar–H), 8.37 (d, J = 4.0 Hz, 1H, thiophene-H), 8.78 (s, 2H, NH_2, D_2O exchangeable); ^{13}CNMR (δ, ppm) 79.40 (C–CN), 113.36 (CN), 113.90 (CN), 116.71, 118.95, 119.36, 122.28, 122.58, 124.41, 127.21, 127.86, 128.62, 134.95, 138.20, 138.71, 139.08 (Ar–Cs), 158.91 (C=N), 162.17 (C–NH_2), 164.51 (CO), 168.51 (CO); anal. calcd. For $C_{20}H_9N_5O_3S$ (399.38): C, 60.15; H, 2.27; N, 17.54. Found: C, 59.81.52; H, 2.11; N, 17.11.

*4.2.1.2.10 6-Amino-1-((1,3-dioxo-1,3-dihydro-2H-inden-2-ylidene)amino)-4-(furan-2-yl)-2-oxo-1,2-dihydropyridine-3,5-dicarbonitrile (**6b**).* M.p.: 305–307 °C; black powder; yield 66% (89%); IR (KBr): ν_{max} 3374, 3313 (NH_2), 3145 (aromatic-H), 2213 (CN), 1723, 1670 (2CO), 1650 (C=N); ^{1}H NMR (δ, ppm) 7.25 (t, J = 4.0 Hz, 1H, furan-H), 7.39 (t, J = 4.0 Hz, 1H, furan-H), 7.51 (d, J = 7.2 Hz, 1H, Ar–H), 7.81 (d, J = 3.1 Hz, 1H, furan-H), 7.91 (d, J = 7.7 Hz, 1H, Ar–H), 8.11 (d, J = 6.2 Hz, 1H, Ar–H), 8.34 (d, J = 7.8 Hz, 1H, Ar–H), 8.47 (s, 2H, NH_2, D_2O exchangeable); ^{13}CNMR (δ, ppm) 81.56 (C–CN), 112.61 (CN), 114.81 (CN), 115.47, 119.89, 120.52, 123.70, 124.68, 127.49, 128.91, 129.48, 130.42, 137.50, 138.54, 139.54, 141.09 (Ar–Cs), 157.32 (C=N), 161.08 (C–NH_2), 162.83 (CO), 166.95 (CO); anal. calcd. For $C_{20}H_9N_5O_4$ (383.32): C, 62.67; H, 2.37; N, 18.27. Found: C, 62.41.52; H, 2.06; N, 17.91.

*4.2.1.2.11 6-Amino-2-oxo-1-((2-oxoindolin-3-ylidene)amino)-4-(thiophen-2-yl)-1,2-dihydropyridine-3,5-dicarbonitrile (**8a**).* M.p.: 258–260 °C; brown powder; yield 76% (94%); IR (KBr): ν_{max} 3389, 3286 (NH_2, NH), 3115 (aromatic-H), 2208 (CN), 1729, 1637 (2CO), 1599 (CH = N); ^{1}H NMR (δ, ppm) = 6.78 (t, J = 4.9 Hz, 1H, thiophene-H), 6.89 (d, J = 3.2 Hz, 1H, thiophene-H), 7.06 (t, J = 7.6 Hz, 1H, Ar–H), 7.33 (d, J = 3.6 Hz, 1H, thiophene-H), 7.48 (t, J = 7.2 Hz, 1H, Ar–H), 7.56 (d, J = 8.0 Hz, 2H, Ar–H), 8.4 (s, 2H, NH_2, D_2O exchangeable), 11.02 (s, 1H, NH-isatin, D_2O exchangeable); ^{13}CNMR (δ, ppm) 75.34 (C–CN), 109.15 (CN), 114.10 (CN), 114.28, 118.68, 119.01, 121.62, 122.87, 126.94, 129.71, 137.87, 142.63, 143.02, 145.54, 147.79 (Ar–Cs), 155.08 (C=N), 159.49 (NH_2), 166.09 (CO), 172.12 (CO); anal. calcd. For $C_{19}H_{10}N_6O_2S$ (386.39): C, 59.06; H, 2.61; N, 21.75. Found: C, 58.61.; H, 2.31; N, 21.21.

*4.2.1.2.12 6-Amino-4-(furan-2-yl)-2-oxo-1-((2-oxoindolin-3-ylidene)amino)-1,2-dihydropyridine-3,5-dicarbonitrile (**8b**).* M.p.: 270–272 °C; brown powder; yield 71% (91%); IR (KBr): ν_{max} 3374, 3313 (NH_2, NH), 3045 (aromatic-H), 2213 (CN), 1723, 1670 (2CO), 1650 (CH = N); ^{1}H NMR (δ, ppm) = 6.84 (t, J = 4.8 Hz, 1H, furan-H), 6.89 (d, J = 3.6 Hz, 1H, furan-H), 7.15 (t, J = 8.0 Hz, 1H, Ar–H), 7.38 (d, J = 4.8 Hz, 1H, furan-H), 7.47 (t, J = 7.2 Hz, 1H, Ar–H), 7.62 (d, J = 8.0 Hz, 2H, Ar–H), 8.06 (s, 2H, NH_2, D_2O exchangeable), 11.61 (s, 1H, NH-isatin, D_2O exchangeable); ^{13}C NMR (δ, ppm) 78.11(C–CN), 112.66 (CN), 114.28 (CN), 114.33, 117.15, 118.85, 120.16, 122.31, 125.31, 128.11, 136.87, 140.38, 141.11, 144.25, 147.10 (Ar–Cs), 151.55 (C=N), 158.28 (NH_2), 164.82 (CO), 171.16 (CO); anal. calcd. For $C_{19}H_{10}N_6O_3$ (370.32): C, 61.62; H, 2.72; N, 22.69. Found: C, 61.41; H, 2.31; N, 22.43.

4.2.2. Synthesis of the target tetracyclic compounds (7a,b and 9a,b)

4.2.2.1 Method (a). To a solution of pyridine Schiff base derivatives **6a,b** (0.01 mmol) or **8a,b** (0.01 mmol) dimethylformamide (10 mL) as a solvent was heated under reflux for 17–20 h (monitoring by TLC). After the reaction is completed, the solution mixture was added to 20 mL cold ethanol, and the precipitated solid was filtered, washed with ethanol, dried, and crystallized from ethanol to yield the desired compounds.

4.2.2.2 Method (b). To a solution of pyridine Schiff base derivatives **6a,b** (0.01 mmol) or **8a,b** (0.01 mmol) and cerium ammonium nitrate (2 mol%), was dissolved in acetonitrile (5 mL), the solution was stirred at room temperature for 4–5 h (monitoring by TLC). After the reaction is completed, the solid product that precipitated was filtered out, washed with ethanol, dried, and crystallized from ethanol to produce the desired compounds with high yield.

4.2.2.3 Method (c). The 1,6-diamino-pyridine derivatives **1a,b** (0.01 mol), and ninhydrin or isatin (1 mmol) were dissolved in DMF (10 mL), the solution was heated under reflux for 17–20 h (monitoring by TLC). After the reaction is completed, the mixture was added to 20 mL cold ethanol, and the precipitated solid was filtered, washed with ethanol, dried, and crystallized from ethanol.

4.2.2.4 Method (d). The 1,6-diamino-pyridine derivatives **1a,b** (0.01 mol), ninhydrin or isatin (1 mmol), and cerium ammonium nitrate (2 mol%), were dissolved in acetonitrile (5 mL), the solution was stirred at room temperature for 4–5 h (monitoring by TLC). After the reaction is completed, the solid product that precipitated was filtered out, washed with ethanol, dried, and crystallized from suitable solvent to produce the desired compounds with high yield.

*4.2.2.4.1 4,7-Dioxo-2-(thiophen-2-yl)-4,7dihydroindeno[1,2-e] pyrido[1,2-b][1,2,4]triazine-1,3-dicarbonitrile (**7a**).* M.p.: 362–365 °C; brownish powder; yield 69% (91); IR (KBr): ν_{max} 3092 (aromatic-H), 2212 (CN), 1740, 1683 (2CO), 1642 (C=N); ^{1}H NMR (δ, ppm) = 7.42 (t, J = 4.3 Hz, 1H, thiophene-H), 7.82 (d, J = 2.7 Hz, 2H, thiophene-H), 8.15–8.12 (m, 2H, Ar–H), 8.20 (d, J = 7.7 Hz, 1H, Ar–H), 8.36 (d, J = 6.8 Hz, 1H, Ar–H); ^{13}CNMR (δ, ppm) 91.50, 99.17 (2C–CN), 114.68, 115.67 (2CN), 125.70, 125.99, 128.78, 132.47, 133.16, 133.23, 137.16, 138.16, 138.56, 141.06, 148.28, 151.57, 153.09 (Ar–Cs), 156.20 (C=N), 160.58 (CO), 183.62 (CO); anal. calcd. For $C_{20}H_7N_5O_2S$ (381.37): C, 62.99; H, 1.85; N, 18.38. Found: C, 62.61.52; H, 1.78; N, 17.81.

*4.2.2.4.2 4,7-Dioxo-2-(furan-2-yl)-4,7dihydroindeno[1,2-e]pyrido[1,2-b][1,2,4]triazine-1,3-dicarbonitrile (**8b**).* M.p.: 352–354 °C; blue brown powder; yield 71% (84%); IR (KBr): ν_{max} = 3092 (aromatic-H), 2211 (CN), 1647 (CO), 1607 (C=N); ^{1}H NMR (δ, ppm) 7.25 (t, J = 3.6 Hz, 1H, furan-H), 7.39 (t, J = 4.8 Hz, 1H, Ar–H), 7.51 (d, J = 3.2 Hz, 1H, furan-H), 7.80 (d, J = 4.0 Hz, 1H, furan-H), 7.71 (d, J = 5.6 Hz, 1H, Ar–H), 8.1 (t, J = 5.6 Hz, 1H, Ar–H) 8.21 (d, J = 8.4 Hz, 1H, Ar–H); ^{13}CNMR (δ, ppm) 89.80, 97.93 (2C–CN), 113.48, 115.20 (2CN), 124.34, 125.34, 127.90, 131.95, 132.93, 135.57, 137.46, 138.33, 139.78, 141.66, 147.20, 149.37, 152.17 (Ar–Cs), 155.56 (C=N), 158.47 (CO), 175.49 (CO); anal. calcd. For $C_{20}H_7N_5O_3$ (365.30): C, 65.76; H, 1.93; N, 19.17. Found: C, 65.61, H, 1.78; N, 18.81.

*4.2.2.4.3 7-Oxo-9-(thiophen-2-yl)-7,12-dihydropyrido[1′,2′:2,3] [1,2,4]triazino[5,6-b]indole-8,10-dicarbonitrile (**9a**).* M.p.: 301–303 °C; brown powder; yield 65% (85%). IR (KBr): ν_{max} = 3173 (NH), 3095 (aromatic-H), 2213 (CN), 1647 (CO), 1617 (C=N); ^{1}H NMR (δ, ppm) = 7.08 (t, J = 9.2 Hz, 1H, Ar–H), 7.33 (d, J = 3.6 Hz, 2H, thiophene-H), 7.48 (d, J = 7.2 Hz, 1H, Ar–H), 7.58 (t, J = 4.0 Hz, 1H, thiophene-H), 7.77 (d, J = 8.0 Hz, 1H, Ar–H), 7.88 (d, J = 8.0 Hz, 1H, Ar–H), 11.79 (s, 1H, NH-isatin, D_2O exchangeable). ^{13}CNMR (δ, ppm) = 85.48 (C–CN), 114.45, 115.21 (CN), 115.88 (CN), 117.16, 124.10, 126.62, 129.00, 131.19, 132.12, 135.70, 137.47, 139.08, 141.35, 144.29, 151.85 (Ar–Cs), 156.35, 163.69 (C=N), 168.83 (CO); anal. calcd. For $C_{19}H_8N_6OS$ (368.37): C, 61.95; H, 2.19; N, 22.81. Found: C, 61.61.; H, 2.01; N, 22.41.

*4.2.2.4.4 9-(Furan-2-yl)-7-oxo-7,12-dihydropyrido[1′,2′:2,3] [1,2,4]triazino[5,6-b]indole-8,10-dicarbonitrile (**9b**).* M.p.: 310–312 °C; black brown powder; yield 61% (85%); IR (KBr): ν_{max} = 3210 (NH), 2213 (CN), 1723, 1716 (2CO), 1621 (C=N); ^{1}H NMR (δ, ppm) 6.81 (t, J = 3.7 Hz, 1H, furan-H), 6.90 (d, J = 8.0 Hz, 1H, Ar–H), 7.11 (t, J = 8.0 Hz, 1H, Ar–H), 7.33 (d, J = 4.0 Hz, 2H, furan-H), 7.49 (d, J = 8.0 Hz, 1H, Ar–H), 7.58 (t, J = 6.8 Hz, 2H, Ar–H), 11.03 (s, 1H, NH, D_2O exchangeable); ^{13}CNMR (δ, ppm) = 83.53 (C–CN), 115.21 (CN), 115.88 (CN), 116.07, 116.41, 117.87, 125.56, 128.26, 129.55, 132.12, 135.70, 137.47, 140.28, 142.31, 148.18 (Ar–Cs), 154.41 (C=N), 157.44 (C=N), 161.85 (C–NH), 165.94 (2CO); anal. calcd. For $C_{19}H_8N_6O_2$ (351.31): C, 64.77; H, 2.29; N, 23.85. Found: C, 64.41; H, 2.11; N, 22.99.

4.3. Biological evaluation

4.3.1. Microorganisms. The microorganisms used in this work can be classified as: two Gram-positive, four Gram-negative bacterial strains, and one fungal pathogen. Methicillin-sensitive *S. aureus* (MSSA) (ATCC-43300), and Methicillin-resistant *S. aureus* (MRSA) (ATCC-25923) were chosen as Gram-positive bacteria. Among Gram-negative bacteria, *E. coli* (ATCC-25922) and *K. pneumoniae* (ATCC-700603) were selected as Enterobacteriaceae, *P. aeruginosa* (ATCC-2785), and *Acinetobacter baumannii* (ATCC-19606) were selected as non-Enterobacteriaceae. Also, *Candida albicans* (ATCC-10231) were selected to represent fungi.

4.3.2. Agar well diffusion method. The *in vitro* evaluation of all synthesized sixteen compounds was evaluated against seven standard microbial strains using the agar well diffusion method.[74] The steps were conducted at the microbiology lab, faculty of pharmacy (girls), Al-Azhar University, Cairo, Egypt. In this method, 0.5 McFarland (1.5×10^8 CFU mL^{-1}) of microbial isolates were spread on the whole surface of Muller–Hinton agar plates for bacteria and Sabaraud's Dextrose agar for fungi (*C. albicans*). Then, a hole is punched aseptically with a sterile corkborer with a diameter of 8 mm, then a volume (100 mL) of each synthesized compound (at 0.75 mg mL^{-1}) is introduced into the corresponding well. Gentamicin, as well as Fluconazole, were utilized as the antibacterial and antifungal positive control, respectively. As compounds were solubilized in DMSO, DMSO alone was used as a negative control. Plates are incubated 24 h at 37 °C. The procedure was conducted three times for every compound, and their average was recorded as the final reading. After incubation, the average inhibition zone was measured in millimeters and used to indicate antimicrobial activity. Next to the agar well diffusion technique, the most active compounds **2a**, **2b**, **3a**, **3b**, **6a**, and **6b** were selected for further following screening methods.

4.3.3. Minimum inhibitory concentration (MIC). Broth microdilution is one of the most basic antimicrobial susceptibility testing methods. As illustrated by Clinical and Laboratory Standards Institute Guidelines,[75,76] two-fold dilutions of the antimicrobial agent were prepared (1000, 500, 250, 125, 62.5, 31.25, 15.6, 7.8, 3.9, 1.9, 0.9 μg mL^{-1}) in a liquid growth medium. A volume of 100 μL of Muller–Hinton broth media for bacteria or tryptic soy broth for fungi was dispensed in 96-well microtitration plate. Then, 5 μL of a microbial inoculum, adjusted to 0.5 McFarland scale, was introduced into each well. The microtitration plate after well mixing are incubated at conditions compatible with the test microorganism. For every case, examinations were conducted three times, and their average was recorded as the final reading.[74]

4.3.4. Minimum bactericidal/fungicidal (MBC/MFC) concentration. The most prevalent estimate of bactericidal or fungicidal activity is the determination of minimum bactericidal concentration (MBC). It is defined as the least concentration of antimicrobial agent required to kill 99.9% of the microbial inoculum after incubation for 24 h. As described by in document M26-A of CLSI, it is determinable by sub-culturing a sample (about 10 μL) from wells showing a negative growth in broth microdilution test on BD Bacto™ Tryptic soy broth. After 24 h incubation at 37 °C, the number of surviving cells (CFU mL^{-1}) is determined.[74,75]

4.3.5. Antibiofilm activity of the synthesized compounds. The antibiofilm activity of the promising compounds was detected quantitatively by the microtiter plate method. Biofilm formation was measured selectively for MRSA, *P. aeruginosa*, *E. coli*, and *C. albicans*, as they are considered among the most prevalent biofilm producing pathogens. In this procedure, each well of a 96 well-flat bottom polystyrene tissue culture plate (Sigma-Aldrich Co. LLC, USA) was inoculated with 100 μL of the microbial suspension in Muller–Hinton broth with a density of 10^8 CFU mL^{-1}. Subsequently, 100 μL of sub-MIC of the synthesized compounds (1/2, 1/4, 1/8 MICs) of each compound was further added to each well. Then plates are incubated for 24 h at 37 °C. After incubation, the plate content was removed, and the wells were washed with 250 μL phosphate buffer saline PBS (pH 7.4) for three times, then fixed by drying at 60 °C for 1 h. Next, the wells are stained with 200 μL of 0.1% w/v crystal violet (CV) for 15 min.[21,77] The plates were washed repeatedly with distilled water and allowed to dry. The wells were resolubilized with 200 μL of 33% acetic acid. The optical density of each well was measured using a microplate reader at 630 nm (Tecan Elx800, USA). The test was performed in triplicate, and the average was used for further calculations.[23,78] To quantify the biofilm inhibition percentage of synthesized compounds, the following formula was used:[79]

$$\% \text{ inhibition} = 1 - (\text{OD sample/OD positive control}) \times 100$$

4.3.6. Effect of the synthesized compounds on the quorum sensing of *P. aeruginosa*. Quantitative real-time PCR was used to evaluate the efficacy of synthesized compounds' 1/8 MIC to downregulate the expression of the LasR gene.

4.3.6.1 RNA extraction and conversion to DNA. Total RNA was isolated from *P. aeruginosa* (ATCC 2785) using the First High Pure RNA Isolation Kit (Cat. No. 11 828 665001, Roche Diagnostics GmbH, Germany) in accordance with the manufacturer's instructions. Using the QuantiTects Reverse Transcription Kit, one g of total RNA was reverse-transcribed into single-stranded complementary DNA (Qiagen, USA).[80]

4.3.6.2 Quantitative RT-PCR of lasR gene. RT-PCR was performed in two steps with a random primer hexamer, and any genomic DNA (gDNA) contamination was removed with gDNA wipeout buffer. Total cDNA (30 ng) was used as a template for amplification with the specific primers pair *via* Maxima SYBR Green/Fluorescein qPCR Master Mix. The forward and reverse gene-specific PCR primers for LasR were (5′-CTGTGGATGCTCAAGGACTAC-3′) and (5′-AACTGGTCTTGCCGATGG-3′), respectively. ropD was used as reference gene of primers' sequences of 5′-CGAACTGCTTGCCGACTT-3′ and 5′-GCGAGAGCCTCAAGGATAC-3′ for forward and reverse, respectively. Additionally, the sample was subjected to real-time PCR in duplicate and the mean values of the duplicates were used for subsequent analysis. Data was calculated using ΔΔCt method to estimate relative gene expression where fold change equal to $(2^{-\Delta\Delta ct})$.[80,81]

4.3.7. Cytotoxicity/viability assay. The MTT assay on Vero cells (normal cell line) was used to evaluate the cytotoxicity of the synthesized compounds. In this approach, the number of active cells is determined by how well they can use a reduction reaction that occurs in the mitochondria to turn the yellow product MTT into the blue result, formazan. 1×10^5 cells per mL (100 μL per well) were used to inoculate the 96-well tissue culture plate. The growth medium was decanted from plates after 24 h of incubation and the creation of a confluent sheet of cells, and the cell monolayer was then twice washed with wash media. Following this, two-fold dilutions of the tested compounds were prepared in RPMI medium with 2 percent serum, and 0.1 mL of each dilution was tested in various wells, leaving 3 wells as controls that merely received maintenance media. Cells were examined for any physical toxicity indicators after being incubated at 37 °C, such as partial or full loss of the monolayer, rounding, shrinkage, or cell granulation. Then, plates were put on a shaking table with 20 L of MTT solution added to each well. The medium was discarded, and 200 μL of DMSO was added to resuspend formazan (MTT metabolic product). Finally, the background was subtracted at 620 nm while optical density was measured at 560 nm. The number of cells and optical density would be closely connected.[82,83]

4.4. The docking simulation

The docking simulation of the most active 2-oxo-pyridine derivatives was performed inside the active site of LasR protein. The crystal structure (PDB ID: 6MVN) involved two chains and our docking process was carried out using only one chain (chain A) and all water molecules and other ligand were deleted. The docking process was performed using Molecular Operating Environment (MOE) version 2014.0901.[84–86] The co-crystallized 3-oxo-*N*-[(3S)-2-oxotetrahydrofuran-3-yl] decanamide was redocked inside the active site that generated under default parameters and exhibited binding energy $S = -9.3504$ kcal mol^{-1} and RMSD = 0.6986 Å, where the triangle matcher was selected as replacement and London dG as rescoring 1 with fifty retain and forcefield as refinement. The self-docking showed that co-crystallized ligand formed three hydrogen bond sidechain acceptors between Tyr56 and Ser129 with oxygen of carbonyl of amide group with bond length 1.68 and 1.97 Å and the third bond presented between the residue Trp60 with the oxygen of furanone derivatives with bond length of 2.19 Å. Additionally, the residue Asp73 bounded to NH of amide at C3 of furane derivative with hydrogen bond sidechain donor with bond length of 1.74 Å. Besides, the arene–H interaction was observed between the hydrogen of C5 on furane moiety and Trp60.

Conflicts of interest

The authors declare no conflicts of interest.

Acknowledgements

The authors extend their appreciation to the Deanship of Scientific Research at King Khalid University for funding this work through a large group Research Project under grant number RGP2/50/44.

References

1 T. A. Hafiz, S. S. Alghamdi, M. A. Mubaraki, S. S. M. Alghamdi, A. Alothaybi, E. Aldawood and F. Alotaibi, *J. Infect. Public Health*, 2023, **16**, 313–319.

2 L. Yin, Y. Gou, Y. Dai, T. Wang, K. Gu, T. Tang, S. Hussain, X. Huang, C. He, X. Liang, G. Shu, F. Xu and P. Ouyang, *Int. J. Mol. Sci.*, 2023, **24**, 9288.

3 G.-F. Zhang, S. Zhang, B. Pan, X. Liu and L.-S. Feng, *Eur. J. Med. Chem.*, 2018, **143**, 710–723.

4 P. Dadgostar, *Infect. Drug Resist.*, 2019, 3903–3910.

5 N. Nagasundaram, K. Padmasree, S. Santhosh, N. Vinoth, N. Sedhu and A. Lalitha, *J. Mol. Struct.*, 2022, **1263**, 133091.

6 E. R. A. Mahmoud, H. A. H. Ahmed, A. S. M. Abo-senna, O. K. M. Riad and M. M. A. A. – R. A.- Shadi, *J. Radiat. Res. Appl. Sci.*, 2021, **14**, 34–43.

7 E. Leemans, K. V Mahasenan, M. Kumarasiri, E. Spink, D. Ding, P. I. O'Daniel, M. A. Boudreau, E. Lastochkin, S. A. Testero and T. Yamaguchi, *Bioorg. Med. Chem. Lett.*, 2016, **26**, 1011–1015.

8 A. Ragab, Y. A. Ammar, A. Ezzat, A. M. Mahmoud, M. Basseem, I. Mohamed, A. S. El-tabl and R. S. Farag, *Comput. Biol. Med.*, 2022, **145**, 105473.

9 A. Ezzat, M. B. I. Mohamed, A. M. Mahmoud, R. S. Farag, A. S. El-Tabl and A. Ragab, *J. Mol. Struct.*, 2022, **1251**, 132004.

10 P. A. Akinduti, O. W. George, H. U. Ohore, O. E. Ariyo, S. T. Popoola, A. I. Adeleye, K. S. Akinwande, J. O. Popoola, S. O. Rotimi, F. O. Olufemi, C. A. Omonhinmin and G. I. Olasehinde, *Antibiotics*, 2023, **12**, 626.

11 R. Chen, G. Wang, Q. Wang, M. Zhang, Y. Wang, Z. Wan, Z. Si, Y. Bai, Z. Song, X. Lu and Y. Hao, *Int. J. Microbiol.*, DOI: 10.1007/s10123-023-00369-7.

12 V. Zammuto, A. Spanò, E. Agostino, A. Macrì, C. De Pasquale, G. Ferlazzo, M. G. Rizzo, M. S. Nicolò, S. Guglielmino and C. Gugliandolo, *Mar. Drugs*, 2023, **21**, 313.

13 A. Ragab, S. A. Fouad, Y. A. Ammar, D. S. Aboul-Magd and M. S. Abusaif, *Antibiotics*, 2023, **12**, 128.

14 Y. A. Ammar, J. A. Micky, D. S. Aboul-Magd, S. M. A. Abd El-Hafez, S. A. Hessein, A. M. Ali and A. Ragab, *Chem. Biol. Drug Des.*, 2023, **101**, 245–270.

15 M. M. Abdelgalil, Y. A. Ammar, G. A. M. Elhag Ali, A. K. Ali and A. Ragab, *J. Mol. Struct.*, 2023, **1274**, 134443.

16 R. Rezende Mires de Carvalho, C. Silva Dias, L. Nogueira Paz, T. Melo de Lima Fires, C. Pereira Figueira, K. Araújo Damasceno and M. Hanzen Pinna, *Heliyon*, 2023, **9**, e13802.

17 T. Yamaguchi, N. Higa, N. Okura, A. Matsumoto, I. Hermawan, T. Yamashiro, T. Suzuki and C. Toma, *BMC Microbiol.*, 2018, **18**, 64.

18 A. A. N. Santos, C. P. Figueira, M. G. dos Reis, F. Costa and P. Ristow, *Braz. J. Microbiol.*, 2015, **46**, 1161–1164.

19 W. Mousa, N. Omar, O. K. M. Riad and M. E. A. Omran, *Azhar International Journal of Pharmaceutical and Medical Sciences*, 2022, **2**, 94–104.

20 P. Pachori, R. Gothalwal and P. Gandhi, *Genes Dis.*, 2019, **6**, 109–119.

21 M. S. E. M. Badawy, O. K. M. Riad, F. A. Taher and S. A. Zaki, *Int. J. Biol. Macromol.*, 2020, **149**, 1109–1117.

22 E. P. Perikleous, D. Gkentzi, A. Bertzouanis, E. Paraskakis, A. Sovtic and S. Fouzas, *Antibiotics*, 2023, **12**, 217.

23 A. Y. Alzahrani, Y. A. Ammar, M. Abu-Elghait, M. A. Salem, M. A. Assiri, T. E. Ali and A. Ragab, *Bioorg. Chem.*, 2022, **119**, 105571.

24 O. Kindler, O. Pulkkinen, A. G. Cherstvy and R. Metzler, *Sci. Rep.*, 2019, **9**, 12077.

25 V. Bettenworth, B. Steinfeld, H. Duin, K. Petersen, W. R. Streit, I. Bischofs and A. Becker, *J. Mol. Biol.*, 2019, **431**, 4530–4546.

26 S. Mukherjee and B. L. Bassler, *Nat. Rev. Microbiol.*, 2019, **17**, 371–382.

27 S. S. Chourasiya, D. Kathuria, S. Singh, V. C. Sonawane, A. K. Chakraborti and P. V Bharatam, *RSC Adv.*, 2015, **5**, 80027–80038.

28 S. Park, H.-S. Kim, K. Ok, Y. Kim, H.-D. Park and Y. Byun, *Bioorg. Med. Chem. Lett.*, 2015, **25**, 2913–2917.

29 S. Nizalapur, Ö. Kimyon, N. N. Biswas, C. R. Gardner, R. Griffith, S. A. Rice, M. Manefield, M. Willcox, D. S. Black and N. Kumar, *Org. Biomol. Chem.*, 2016, **14**, 680–693.

30 M. E. Skindersoe, M. Alhede, R. Phipps, L. Yang, P. O. Jensen, T. B. Rasmussen, T. Bjarnsholt, T.-N. Tim, T. Tolker-Nielsen, N. Høiby and M. Givskov, *Antimicrob. Agents Chemother.*, 2008, **52**, 3648–3663.

31 M. Kurva, S. G. Pharande, A. Quezada-Soto and R. Gámez-Montaño, *Tetrahedron Lett.*, 2018, **59**, 1596–1599.

32 A. K. Gunthanakkala, M. S. Mangali, P. Venkatapuram and P. Adivireddy, *J. Heterocycl. Chem.*, 2020, **57**, 4164–4174.

33 M. A. Ismail, M. S. Abusaif, M. S. A. El-Gaby, Y. A. Ammar and A. Ragab, *RSC Adv.*, 2023, **13**, 12589–12608.

34 R. Ayman, M. S. Abusaif, A. M. Radwan, A. M. Elmetwally and A. Ragab, *Eur. J. Med. Chem.*, 2023, **249**, 115138.

35 K. Harada, T. Ferdous, T. Harada, T. Takenawa and Y. Ueyama, *Oncol. Lett.*, 2017, **14**, 3349–3356.

36 R. I. Sanchez, K. L. Fillgrove, K. L. Yee, Y. Liang, B. Lu, A. Tatavarti, R. Liu, M. S. Anderson, M. O. Behm and L. Fan, *Xenobiotica*, 2019, **49**, 422–432.

37 T. S. U. Sihotang, A. D. W. Widodo and P. D. Endraswari, *Ann. Med. Surg.*, 2022, **82**, 104674.

38 F.-A. Khan, S. Yaqoob, S. Ali, N. Tanveer, Y. Wang, S. Ashraf, K. A. Hasan, S. A. M. Khalifa, Q. Shou, Z. Ul-Haq, Z.-H. Jiang and H. R. El-Seedi, *Molecules*, 2023, **28**, 212.

39 A. Ragab, S. A. Fouad, O. A. A. Ali, E. M. Ahmed, A. M. Ali, A. A. Askar and Y. A. Ammar, *Antibiotics*, 2021, **10**, 162.

40 A. K. Bass, E. Abdelhafez, M. El-Zoghbi, M. F. A. Mohamed, M. Badr and G. E.-D. A. A. Abuo-Rahma, *J. Adv. Biomed. Pharm. Sci.*, 2021, **4**, 81–86.

41 H. A. Soliman, A. H. Shamroukh, E. R. Kotb, K. Mahmoud, E. H. Anouar and M. I. Hegab, *J. Mol. Struct.*, 2022, **1263**, 133148.

42 A. M. Al-Etaibi and M. A. El-Apasery, *Int. J. Environ. Res. Public Health*, 2020, **17**, 4714.

43 R. Alasbahi and M. Melzig, *Sci. Pharm.*, 2008, **76**, 471–484.

44 A. M. Attia, A. I. Khodair, E. A. Gendy, M. A. El-Magd and Y. A. M. M. Elshaier, *Lett. Drug Des. Discovery*, 2020, **17**, 124–137.
45 N. M. A. Gawad, H. H. Georgey, R. M. Youssef and N. A. El-Sayed, *Eur. J. Med. Chem.*, 2010, **45**, 6058–6067.
46 N. Ryad, A.-S. My, M. M. Ismail and S. El Meligie, *Chem. Pharm. Bull.*, 2018, **66**, 939–952.
47 L. K. A. Karem, F. Y. Waddai and N. H. Karam, *J. Pharm. Sci. Res.*, 2018, **10**, 1912–1917.
48 Y. Toubi, F. Abrigach, S. Radi, F. Souna, A. Hakkou, A. Alsayari, A. Bin Muhsinah and Y. N. Mabkhot, *Molecules*, 2019, **24**, 3250.
49 T. Tunc, A. B. Ortaakarsu, S. M. Hatipoglu, U. Kazancı, S. Karabocek, N. Karabocek, N. Dege and N. Karacan, *J. Mol. Struct.*, 2022, **1254**, 132299.
50 K.-C. Gan, K.-M. Sim, T.-M. Lim and K.-C. Teo, *Lett. Org. Chem.*, 2020, **17**, 191–198.
51 S. Javad, E. Samane, T. Raheleh and S. Hossein, *Org. Prep. Proced. Int.*, 2019, 1–9.
52 M. Tahmasby, A. Darehkordi, M. Mohammadi and F. Nejadkhorasani, *J. Mol. Struct.*, 2021, **1224**, 129032.
53 A. Darehkordi, V. Salehi, F. Rahmani and M. Karimipour, *Int. J. Biol. Macromol.*, 2018, **54**, 554–558.
54 A. A. Ali, H. Abd El-Wahab, M. S. Abusaif, A. Ragab, O. A. Abdel-Jaid, E. A. Eldeeb and Y. A. Ammar, *Pigm. Resin Technol.*, DOI: **10.1108/PRT-12-2022-0141**.
55 A. P. Zarecki, J. L. Kolanowski and W. T. Markiewicz, *Molecules*, 2020, **25**, 1761.
56 M. Kalhor, S. Samiei and S. A. Mirshokraei, *Green Chem. Lett. Rev.*, 2021, **14**(3), 500–508.
57 E. A. Fayed, M. Mohsen, S. M. A. El-Gilil, D. S. Aboul-Magd and A. Ragab, *J. Mol. Struct.*, 2022, **1262**, 133028.
58 H. A. Mohamed, Y. A. Ammar, G. A. M. Elhagali, H. A. Eyada, D. S. Aboul-Magd and A. Ragab, *J. Mol. Struct.*, 2023, **1287**, 135671.
59 K. Zahmatkesh, K. A. Dilmaghani and Y. Sarveahrabi, *Acta Chim. Slov.*, 2022, **69**, 619–628.
60 J. Chadha, Ravi, J. Singh, S. Chhibber and K. Harjai, *Front. Cell. Infect. Microbiol.*, 2022, **12**, 899566.
61 F. M. Husain, I. Ahmad, M. Asif and Q. Tahseen, *J. Biosci.*, 2013, **38**, 835–844.
62 H. Ali Mohamed, Y. A. Ammar, G. A. M. Elhagali, H. A. Eyada, D. S. Aboul-Magd and A. Ragab, *ACS Omega*, 2022, **7**, 4970–4990.
63 P. Awolade, N. Cele, N. Kerru and P. Singh, *Mol. Diversity*, 2021, **25**, 2201–2218.
64 Y. A. Ammar, G. A. M. Elhagali, M. S. Abusaif, M. R. Selim, M. A. Zahran, T. Naser, A. B. M. Mehany and E. A. Fayed, *Med. Chem. Res.*, 2021, **30**, 1649–1668.
65 H. F. Rizk, M. A. El-Borai, A. Ragab, S. A. Ibrahim and M. E. Sadek, *Polycyclic Aromat. Compd.*, 2023, **43**, 500–522.
66 S. A. Ibrahim, A. Ragab and H. A. El-Ghamry, *Appl. Organomet. Chem.*, 2022, **36**, 1–17.
67 A. S. Hassan, N. M. Morsy, W. M. Aboulthana and A. Ragab, *RSC Adv.*, 2023, **13**, 9281–9303.
68 R. R. Raslan, Y. A. Ammar, S. A. Fouad, S. A. Hessein, N. A. M. Shmiess and A. Ragab, *RSC Adv.*, 2023, **13**, 10440–10458.
69 R. Ayman, A. M. Radwan, A. M. Elmetwally, Y. A. Ammar and A. Ragab, *Arch. Pharm.*, 2022, e2200395.
70 E. A. Fayed, A. Ragab, R. R. Ezz Eldin, A. H. Bayoumi and Y. A. Ammar, *Bioorg. Chem.*, 2021, **116**, 105300.
71 A. S. Hassan, N. M. Morsy, W. M. Aboulthana and A. Ragab, *Drug Dev. Res.*, 2023, **84**, 3–24.
72 K. E. Saadon, N. M. H. Taha, N. A. Mahmoud, G. A. M. Elhagali and A. Ragab, *J. Iran. Chem. Soc.*, 2022, **19**, 3899–3917.
73 G. H. Elgemeie and S. H. Sayed, *Synthesis*, 2010, 37–41.
74 M. Balouiri, M. Sadiki and S. K. Ibnsouda, *J. Pharm. Anal.*, 2016, **6**, 71–79.
75 *Methods for Determining Bactericidal Activity of Antimicrobial Agents, Approved Guideline, CLSI document M26-A*, Clinical and Laboratory Standards Institute, 950 West Valley Road, Suite 2500, Wayne, Pennsylvania 19087, USA.
76 M. S. Kamel, M. O. Aboelez, M. R. Elnagar, E. K. Shokr, H. M. R. M. Selim, H. E. Abdel-Ghany, A. M. Drar, A. Belal, M. A. El Hamd and M. Abd El Aleem Ali Ali El-Remaily, *ChemistrySelect*, 2022, **7**, e202203191.
77 F. Silva, S. Ferreira, J. A. Queiroz and F. C. Domingues, *J. Med. Microbiol.*, 2011, **60**(10), 1479–1486.
78 A. Carbone, S. Cascioferro, B. Parrino, D. Carbone, C. Pecoraro, D. Schillaci, M. G. Cusimano, G. Cirrincione and P. Diana, *Molecules*, 2021, **26**(1), 81.
79 Y. Liu, L. Wu, J. Han, P. Dong, X. Luo, Y. Zhang and L. Zhu, *Front. Microbiol.*, 2020, **11**, 617473.
80 M. M. Saleh, H. A. Abbas and M. M. Askoura, *Microb. Pathog.*, 2019, **127**, 31–38.
81 K. J. Livak and T. D. Schmittgen, *Methods*, 2001, **25**, 402–408.
82 A. A. van de Loosdrecht, R. H. J. Beelen, G. J. Ossenkoppele, M. G. Broekhoven and M. M. A. C. Langenhuijsen, *J. Immunol. Methods*, 1994, **174**, 311–320.
83 A. Ismail, A. S. Doghish, B. E. M. Elsadek, S. A. Salama and A. D. Mariee, *Steroids*, 2020, **160**, 108656.
84 M. Eldeeb, E. F. Sanad, A. Ragab, Y. A. Ammar, K. Mahmoud, M. M. Ali and N. M. Hamdy, *Biomedicines*, 2022, **10**, 722.
85 E. S. A. E. H. Khattab, A. Ragab, M. A. Abol-Ftouh and A. A. Elhenawy, *J. Biomol. Struct. Dyn.*, 2022, **40**, 1–19.
86 S. A. El-Kalyoubi, A. Ragab, O. A. Abu Ali, Y. A. Ammar, M. G. Seadawy, A. Ahmed and E. A. Fayed, *Pharmaceuticals*, 2022, **15**(3), 376.